Chapter 2

Heteropanax fragrans (Kesseru) derived catalyst for biodiesel synthesis

2.1 Introduction

Catalyst plays a major role in the cost-effective green synthesis of biodiesel and heterogeneous catalyst derived from waste plant is gaining leading attention worldwide. The prominent efficiency and adequate recyclability are the basic points of emphasis in addition to renewability, cost-effectiveness and environmentally friendliness of the heterogenous catalyst in biodiesel synthesis. Plant-based heterogenous catalyst is a green catalyst. Calcination of the waste plant part or ashes is employed for catalyst preparation and it is stated that suitable calcination temperature generates adequate composition and favourable morphology for effective catalytic activity. In this chapter, preparation, characterization, catalytic performance evaluation of heterogeneous base catalyst derived from *Heteropanax fragrans* (Kesseru) is investigated. The characterization of the produced biodiesel and its fuel property analysis are also included in this chapter.

Heteropanax fragrans (Roxb.) Seem commonly known as Kesseru is an ornamental evergreen plant of the family Araliaceae and is native to Asia. *H. fragrans* is one of the primary food plants for rearing Eri silkworm cultured in the North-eastern part of India for producing high-quality silk for making warm clothes [199,200]. Silk is a symbol of elegance and luxury worldwide and Eri is one of them which is believed to be originated in Assam, India and cultured mainly by the tribal people [200]. Eri silkworms are reared on castor and *H. fragrans* plants in Assam, India. *H. fragrans* leaves are mainly used for large-scale commercial rearing of Eri silkworm in Assam, India [199]. In addition to the usage as a feed for Eri silkworm, *H. fragrans* is also used as a medicinal plant in India and other parts of the world [201–204]. Kalita et al. [201] reported that the juice of Kesseru plant is administered orally for treatment of snake-bite. Similarly, Dohutia et al. [202] stated that the milk leaf of Kesseru is used in the treatment of pneumonia. Jin et al. [203] and Luo et al. [204] studied and reported that the bark of *H. fragrans* has been traditionally prescribed as the herbal tea for the treatment of rheumatism.

Bodo community, one of the major culturally rich tribes of Assam, India, has enormous traditional knowledge in utilizing natural resources as food items and traditional medicines in their day-to-day life. They also have the common practice of preparing *Khardwi* or *Khar*

which is the water-extract of the burnt ash of various waste-plant materials. The ashes are also being used as materials for washing hands and utensils as well as insect repellent in growing crops and the prepared *Khardwi* is being used as a food ingredient [205]. *Musa balbisiana*, *Brassica nigra*, *Sesamum indicum*, etc. are some of the plants which are commonly used in the preparation of alkali (*Khardwi*) [205, 206]. The *Khardwi* prepared by the tribal people is highly alkaline (basic) in nature with relatively high pH value and is commonly used as alkaline food additive to make several traditional dishes. This acts as potential replacement of commercial food additive "SODA" among the tribal people of the region. In the practice of Eri culture and nurturing of Eri silkworm, large quantity of untied *H. fragrans* branches are generated as residues or wastes and the Bodo people living particularly in Udalguri district of Assam, India uses these untied plant parts for the preparation of *Khardwi* from the ash obtained by igniting and burning the dry materials. In this context, it was presumed that the ash of *H. fragrans* plant could be developed as a highly basic and competent solid catalyst for the transformation of triglyceride (oil) to biodiesel through transesterification process. The literature survey on the catalytic application of *H. fragrans* confirms that it has not been reported for any reaction as a catalyst. Hence, the present study was undertaken to explore the potential application of *H. fragrans* derived catalyst for cost-effective and green production of biodiesel from non-edible *Jatropha curcas* oil.

2.2 Materials and methods

2.2.1 Materials

The branches of *H. fragrans* (Kesseru) plants were collected from the Udalguri district of Assam, India in November 2018 for the preparation of ash catalyst. To investigate the efficacy of the prepared catalyst in the biodiesel synthesis reaction, *J. curcas* oil was obtained from the LIFERR^{TM} Naturally Elite (Sinhal Herbs, Madhya Pradesh), India. Methanol (≥ 99.0 %), *n*-hexane (≥ 96.0 %), aniline (≥ 99.5 %), ethyl acetate (≥ 99.5 %), phenolphthalein, bromothymol blue, silica gel G (particle size through BSS 350, ≥ 95 %) and sodium sulphate (anhydrous) (≥ 99.0 %) were obtained from Merck, Mumbai, India. 4-Nitroaniline (99.0 %) was obtained from Loba Chemie, Mumbai, India. Nile blue is obtained from Sisco Research Laboratories, Mumbai, India and benzoic acid from Avantor Performance Materials India Limited. Acetone (≥ 99.0 %) and petroleum ether (40–60 ^{o}C) of analytical grade were bought from Rankem, Maharashtra, India. The required distilled water is prepared in a double distillation apparatus in the university laboratory. All the chemicals were used as received.

2.2.2 Methods

2.2.2.1 Preparation of catalyst

The waste *H. fragrans* plant branches collected were cut into small portions, allowed to dry in the sunlight for about 20 days and then the dried materials were ignited in the open air and burnt into ash. Further, the ashes obtained were calcined at 550 and 850 ^{o}C for 2 h in a furnace (programmable). The burnt ash and the ash materials calcined at 550 and 850 ^{o}C were powdered separately using a mortar grinder and then separately kept in the dry container for investigation of catalytic activity and characterization. A pictorial representation of the preparation of the *H. fragrans* catalyst is depicted in **Fig. 2.1**.

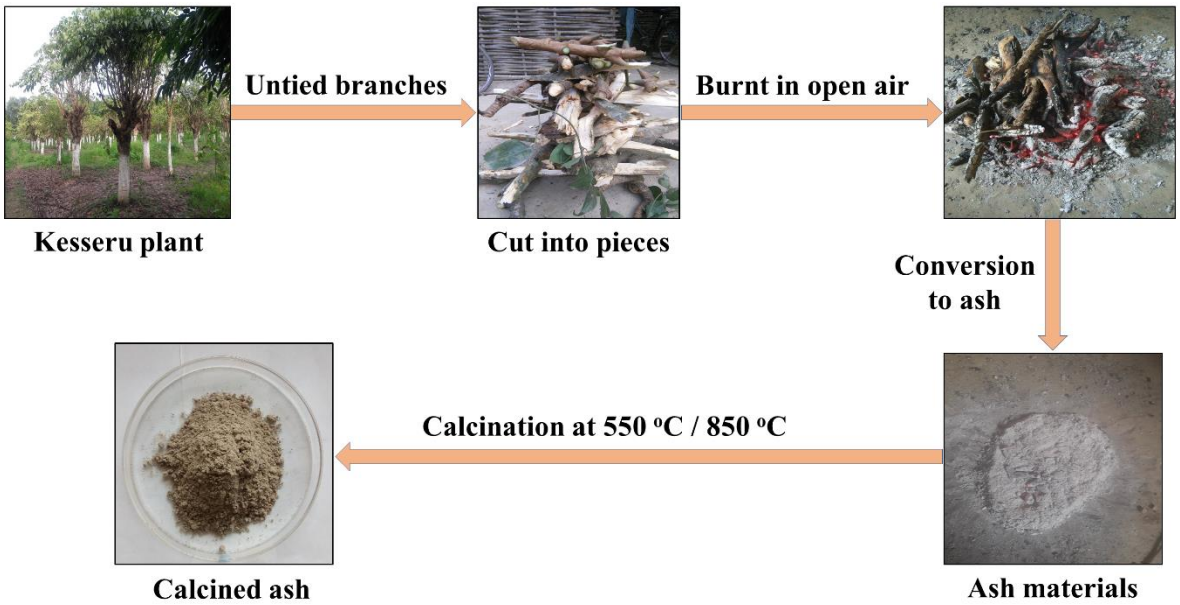

Fig. 2.1. Preparation of *Heteropanax fragrans* catalyst.

2.2.2.2 Catalyst characterization

Bruker AXS X-ray diffractometer (D8 FOUS, Germany) was used to obtain the XRD pattern for the investigation of the qualitative composition of the Kesseru catalyst. Fourier transform infrared (FT-IR) spectra were recorded in the range of 4000 to 400 cm^{-1} using Alpha II Bruker FT-IR spectrometer (410025, Germany). BET (Brunauer-Emmett-Teller), BJH (Barrett-Joyner-Halenda) and N_2 adsorption-desorption isotherm methods were used to measure surface area, pore size distribution and porous characters of the prepared catalyst with the help of Quantachrome instrument (ASiQwin^{TM}, Version 3.0). Field emission scanning electron microscope (Carl Zeiss, SIGMA HV, 05–07, United Kingdom) and Energy dispersive X-ray (EDX) were used to obtain FESEM images and EDX spectra for

investigation of surface morphology and elemental composition of the Kesseru catalysts. Thermo Fischer Scientific X-ray photoelectron spectrometer (ESCALAB Xi^+, USA) was employed to determine the surface composition using the Cu (copper) tape. HRTEM (High resolution transmission electron microscope) images and SAED (Selected area electron diffraction) patterns were recorded using a TEM instrument (JEOL, 200 kV, JEM-2100 plus). The pH values of the Kesseru catalysts were determined by using digital Auto deluxe pH meter (Labtronics, LT-10) by mixing and dissolving the solid catalyst with water (distilled) at six different ratios such as 1:5, 1:10, 1:15, 1:20, 1:30 and 1:40 (w/v). Each solution was prepared by stirring the mixture for few minutes followed by filtration through Whatman no. 1 filter paper. The basicity of *H. fragrans* catalyst was evaluated by Hammett indicator based benzoic acid titration method with slight modification [207]. The indicators used in the present study were 0.02 mol/L methanolic solution of bromothymol blue (H_ = 7.2), phenolphthalein (H_ = 9.3), nile blue (H_ = 10.1), 4-nitroaniline (H_ = 18.4) and aniline (H_ = 27.0). A 100 mg of the *H. fragrans* catalyst was mixed thoroughly with 15 mL of methanol in a 50 mL conical flash and stirred for 1-2 min using the magnetic stirrer. To the catalyst solution mixture, 2-3 drops of indicator was added and stirred for 30 min and then the solution was kept for 15 min so that it reaches to the equilibrium. The appearance of the color in the solution was recorded. Subsequently, the solution was titrated against the 0.01 molar benzoic acid solution prepared in methanol and finally, the basicity (mmol/g) was evaluated from the titre value.

2.2.2.3 Transesterification of *J. curcas* oil and characterization of produced biodiesel

The synthesis of *J. curcas* biodiesel was done by mixing *J. curcas* oil and methanol using the burnt and calcined *H. fragrans* catalysts in the 250 mL two neck flask (round bottomed) fitted to the reflux condenser over a magnetic stirrer. The optimum reaction conditions (ORCs) for the synthesis of biodiesel were investigated by varying the reaction conditions such as methanol to oil ratio (MTOR) (3:1, 6:1, 9:1, 12:1, 15:1 and 18:1) and catalyst concentration (3, 5, 7 and 9 wt.% of oil) at the reaction temperatures of 32 ^oC (room temperature), 45 ^oC, 55 ^oC, 65 ^oC and 75 ^oC. The ideal calcination temperature for the effectiveness of the derived catalyst was investigated by performing the reactions with the BHC (burnt *H. fragrans* catalyst), CC-550 (catalyst calcined at 550 ^oC) and CC-850 (catalyst calcined at 850 ^oC) under the ORCs of 7 wt.% of catalyst dose and 12:1 MTOR at 65 ^oC. The reaction progress was monitored with TLC using the solvent ratio of 1:20 (ethyl acetate and *n*-hexane). After reaction completion, the product (biodiesel) was extracted four times by taking *n*-hexane and 10% NaCl solution in the separating funnel and thereafter, the extracted

solution was dried with Na_2SO_4 (anhydrous) and finally the solvent was concentrated and removed completely at 50 ^oC using a QuickVap evaporator (Almicro). The extracted product was purified through silica gel (60–120 mesh) using the solvent ratio of 1:20 (ethyl acetate and *n*-hexane). The biodiesel yield of the reaction was measured following the equation (2.1).

$$\text{Biodiesel yield (\%)} = \frac{\text{Weight of product}}{\text{Weight of oil}} \times 100 \qquad (2.1)$$

FT-IR spectra of *J. curcas* oil and its biodiesel were obtained from Shimadzu FT-IR spectrometer (MIRacle 10, 00644). Bruker Avance II FT-NMR spectrometer was employed for obtaining ^1H NMR (400 MHz) and ^{13}C NMR (100 MHz) spectra of *J. curcas* oil and produced biodiesel using $CDCl_3$ as the solvent. The methyl ester composition of *J. curcas* biodiesel was determined with the help of Clarus 600 Perkin Elmer GC-MS (Elite 5 MS, split ratio = 20:1, 123.5 m × 678 µm, carrier gas = Helium, mass scan = 20 to 500 Da). During analysis, initially, the oven temperature was kept for 3 min at 90 ^oC, the temperature was raised to 130 ^oC at 10 ^oC/min, it was kept for 3 min and then ramped to 210 ^oC at 10 ^oC/min, kept for 5 min and again the temperature was raised to 280 ^oC at 15 ^oC/min. Properties of *J. curcas* biodiesel such as cetane number, density, pour point, kinematic viscosity and cold filter plugging point were determined at Indian Oil Corporation Limited, Bongaigaon, India. Iodine number (value) and saponification number (value) of *J. curcas* biodiesel were obtained following reported procedures [208,209] and the cetane index, higher heating value (calorific value), diesel index, aniline point and American petroleum index (API) were determined by following the ASTM D2015 standard equations [210].

2.2.2.4 Determination of activation energy and pre-exponential factor

The transesterification process for the synthesis of biodiesel from vegetable oil (triglyceride) with methanol in excess has been reported that follows the kinetics of pseudo-first order reaction [205,211,212]. In this investigation, basic heterogeneous catalyst from Kesseru (*H. fragrans*) was employed for the production of *J. curcas* biodiesel by performing the reaction at various temperatures *viz*. 32 ^oC (room temperature), 45 ^oC, 55 ^oC, 65 ^oC and 75 ^oC. Thereafter, we determined the rate constant of the reaction and then calculated the activation energy (Ea) following the Arrhenius equation [212]. The equation of rate constant for the transesterification reaction is

$$-\ln (1-X_t) = k.t \qquad (2.2)$$

where, X_t is the fraction of FAME obtained in time t and k is the rate constant (min^{-1}).

Following equation (2.2), the value of rate constant at different temperature are determined. The values of activation energy (E_a) and pre-exponential factor (A) were determined from the slopes (= E_a/R, R = 8.314 J K^{-1} $mol^{-}1$, the universal gas constant) and the intercepts (= ln A) of the straight lines of the Arrhenius plots drawn following the Arrhenius equation (2.3) [212].

$$\ln k = - Ea/RT + \ln A \quad (2.3)$$

where, T is the reaction temperature in Kelvin, R is the universal gas constant (8.314 J K^{-1} mol^{-1}) and A is the pre-exponential factor.

2.3 Results and discussion

2.3.1 *H. fragrans* catalyst characterization

2.3.1.1 XRD analysis

The XRD patterns of *H. fragrans* catalysts *viz*. burnt catalyst and the catalysts calcined at 550 and 850 ^oC are depicted in **Fig. 2.2**. Crystalline components present in the catalysts were characterized by comparing the XRD 2θ values with that of JCPDS data (ICDD 2003) and data from reported literature. The analysis resulted to the presence of KCl, K_2CO_3, K_2O, CaO, $CaCO_3$, Fe_2O_3, $MgCO_3$, P_2O_5, Al_2O_3, SiO_2, $CaMg(CO_3)_2$ and Na_2CO_3 in the *H. fragrans* catalysts. The KCl found in the catalyst was characterized by the 2θ values at 28.35, 40.54, 50.14 in the BHC, at 28.36, 40.46, 50.15 in the CC-550 and at 28.35, 40.55, 50.14, 58.68, 66.46, 73.71 in the CC-850. The K_2CO_3 present in the catalyst was characterized by the XRD peaks at 2θ values of 26.68, 29.75, 30.17, 34.16, 41.00 (BHC), 26.65, 29.68, 30.35, 33.86, 41.67 (CC-550) and 26.68, 29.75, 31.58 (CC-850). It is interesting to mention that the high intense peak due to K_2CO_3 at 2θ value of 26.68 in the BHC and at 2θ value of 26.65 in the CC-550 decreases in the XRD pattern (**Fig. 2.2**, red line) of the CC-850 (2θ = 26.68). This might be because of the decrease of carbonate concentration (K_2CO_3) in the catalyst on increasing the calcination temperature (CC-850) which may be due to the conversion of K_2CO_3 to K_2O at the higher temperature. The presence of K_2O in the *H. fragrans* catalyst was shown in the peaks at 2θ values of 25.38, 27.97, 39.48 (BHC), 25.57, 27.89, 39.45, 48.12 (CC-550) and 25.59, 27.92, 66.50 (CC-850). CaO in the *H. fragrans* catalyst was shown by the peaks at 2θ values of 67.72 (BHC), 32.25, 37.00, 55.35, 64.02, 67.72 (CC-550) and 32.58, 37.15 (CC-850). Comparable 2θ values for CaO were also reported in the catalyst derived

from snail shell [213], rice husk [50], *Tamarindus indica* fruit shell [214] and palm oil mill boiler ash [215]. Similarly, the presence of $CaCO_3$ in the catalyst was characterized by the XRD peaks at 2θ values of 23.10, 29.44, 36.54 (BHC), 36.55 (CC-550) and 23.59 (CC-850) which are in accordance with the values reported for the palm oil mill boiler ash catalyst [215] and shrimp shell catalyst [216]. Fe_2O_3 was found to be present in the burnt catalyst (2θ = 33.21) and the CC-550 (2θ = 33.17) and the values are in agreement with the 2θ values of Fe_2O_3 reported in the work of Zeng et al. [217]. The analysis showed the presence of $MgCO_3$ in the BHC with the 2θ values of 33.54, 42.47, 54.84, 68.51, 77.69 and in the CC-550 with the 2θ values of 42.47 and 54.82. The peaks at 2θ values of 20.88 (BHC) and 20.89 (CC-550 and CC-850) in the XRD pattern showed the presence of P_2O_5 in the *H. fragrans* catalyst (**Fig. 2.2**). The peaks at 2θ values of 59.92, 68.32 (BHC), 32.67, 59.95, 68.28 (CC-550) and 32.86 (CC-850) indicated the presence of Al_2O_3 in the catalyst. The existence of SiO_2 in the catalysts was shown by the peaks at 2θ values of 21.28, 25.38 (BHC), 25.58 (CC-550) and 21.41, 25.59 (CC-850). Dolomite, $CaMg(CO_3)_2$, was found to be present in the *H. fragrans* catalysts which was revealed from the peaks at 2θ values of 31.31, 45.81 (BHC), 45.76 (CC-550) and 30.87, 45.24 (CC-850). It is observed that on calcination of ash catalyst at 550 ^oC, no major changes or decrease of peak intensities of K_2CO_3 or $CaCO_3$ is noticed (**Fig. 2.2**) compared to the burnt catalyst because the decomposition of K_2CO_3 and $CaCO_3$ does not take place at this temperature. However, a major changes or intense decrease of peak intensity of K_2CO_3, which may be due to partial decomposition of K_2CO_3 by releasing CO_2, is observed when the catalyst is calcined at 850 ^oC. In addition, low intense peaks of $CaCO_3$ along with K_2CO_3 are also observed in **Fig. 2.2**. This indicated that K_2CO_3 and $CaCO_3$ are not completely decomposed or converted to K_2O and CaO, respectively as because only partial decomposition of these carbonates occurs at 850 ^oC and complete decomposition is expected at higher temperature beyond 850 ^oC. The XRD patterns of the three catalysts (**Fig. 2.2**) reveal that on increasing the calcination temperature, the intensity of peaks of the components containing carbonate decreases. Thus, after calcination at 550 ^oC, the catalyst contains mainly metal carbonates and metal oxides. However, after calcination at 850 ^oC, the material is primarily composed of oxides of metals along with few or small fractions of carbonates (K, Ca) as shown in **Fig. 2.2** (A, red line). It is concluded from the XRD analysis that K is the dominant component in the *H. fragrans* catalysts which is found to be present as K_2CO_3, K_2O and KCl.

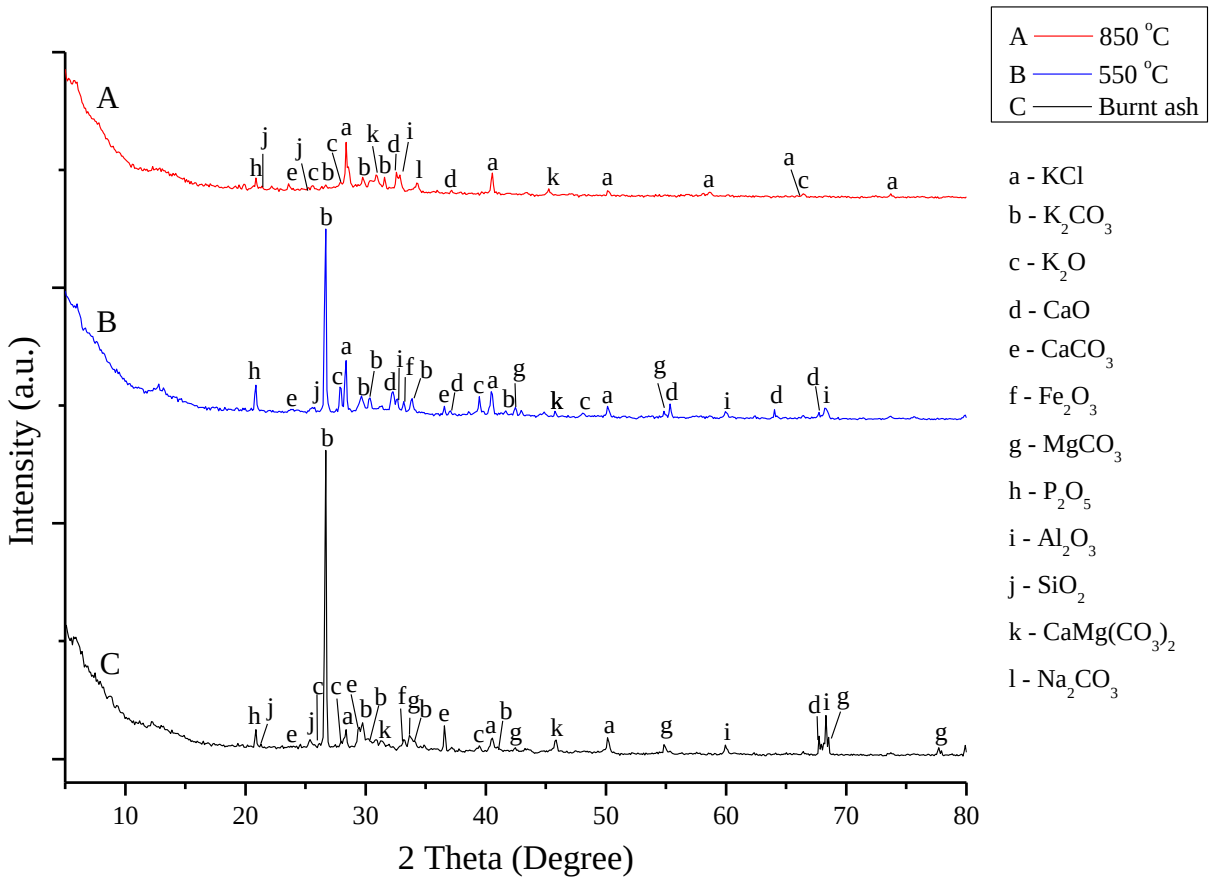

Fig. 2.2. XRD patterns of *H. fragrans* catalysts calcined at 850 °C, 550 °C and burnt ash catalyst.

2.3.1.2 FT-IR study

FT-IR spectra of *H. fragrans* catalysts calcined at 850 °C, 550 °C, 3rd recycled catalyst (550 °C) and BHC are depicted in **Fig. 2.3**. In the spectra of the catalysts, the broad peaks at 3449 cm^{-1} (BHC and CC-850), 3443 cm^{-1} (CC-550) and 3425 cm^{-1} (3rd recycled catalyst) are indicating the stretching frequency of -OH group of H_2O molecules adsorbed on surface of catalyst [206,218,219]. The FT-IR peaks in the spectra of the catalysts at 1639, 1465, 1416, 1384 cm^{-1} (CC-850), 1639, 1462, 1380 cm^{-1} (CC-550), 1645, 1471, 1416 cm^{-1} (3rd recycled catalyst) and 1639, 1459, 1398 cm^{-1} (BHC) are assigning the C–O stretching frequencies due to carbonates of metals (K_2CO_3, $CaCO_3$) present in the catalysts which is supported by XRD analysis (**Fig. 2.2**) and the data are matching with the results of heterogeneous catalysts reported by Betiku et al. [115], Etim et al. [107] and Gohain et al. [220]. The Si–O–Si bond vibrations represented by the peaks at 1116, 1026 cm^{-1} (CC-850), 1120, 1008, 869 cm^{-1} (CC-550), 1116, 1038 cm^{-1} (3rd recycled) and 1116, 1014, 869 cm^{-1} (BHC) of the *H. fragrans* catalysts are in line with the XRD results (**Fig. 2.2**) that revealed the presence of SiO_2 in the

catalysts. The stretching bond vibrations of K–O and Ca–O because of the presence of K_2O and CaO are assigned by the peak at 617 cm^{-1} appeared in the catalysts (BHC, 3rd recycled and CC-550) and at 620 cm^{-1} in the CC-850. In this study, the FT-IR reports of *H. fragrans* catalysts are in conformity with the XRD results which predicted the existence of oxides and carbonates of metals in the catalysts.

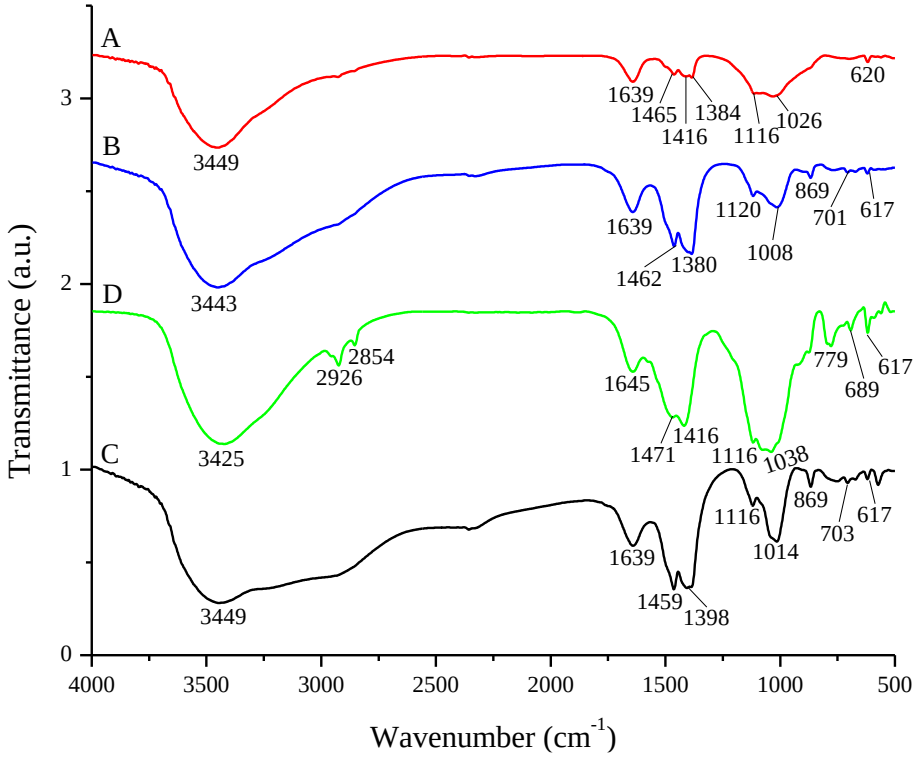

Fig. 2.3. FT-IR spectra of *H. fragrans* catalysts calcined at 850 °C (A), 550 °C (B), burnt ash catalyst (C) and 3rd recycled catalyst (D).

2.3.1.3 Surface area, pore size and pore volume analysis

The physico-chemical properties of the catalysts were measured by BET technique. The BHC, CC-550 and CC-850 showed the appreciable BET surface areas of 57.77, 27.50 and 78.45 m^2 g^{-1} with pore volumes of 0.14, 0.04 and 0.22 cm^3 g^{-1}, respectively. The characteristics of the N_2 adsorption-desorption isotherms of the *H. fragrans* catalysts were found to be similar to the type IV isotherm (**Fig. 2.4** A–C) with H3 isotherm hysteresis loops which are in accordance with Brunauer-Deming-Deming-Teller (BDDT) classification and indicating the existence of mesoporous structure of the catalysts [220–222]. The pore diameters (**Fig. 2.4** D–F) of the BHC and CC-850 were found to be 3.57 and 10.61 nm, respectively which are also in support of their mesoporous structure, whereas the pore diameter of the CC-550 with 1.68 nm indicated the microporous structure of the catalyst [205]. Relatively high surface areas of 38.71 and 39.0 m^2 g^{-1} for *Musa balbisiana* stem

(underground) catalyst were reported by Aslam et al. [110] and Sarma et al. [111], respectively. These catalysts showed comparatively less catalytic activities than that of the present *H. fragrans* catalyst calcined at 550 ^{o}C. Deka and Basumatary [11] and Kumar et al. [197] also reported low catalytic activities of *Musa balbisiana* trunk and *Musa balbisiana* stem (underground) catalysts with very low surface areas of 1.487 and 0.043 m^2 g^{-1} respectively compared to the present catalyst. In recent times in the applications of heterogeneous ash catalysts for the synthesis of biodiesel, Gohain et al. [109] (10.176 m^2 g^{-1}), Wang et al. [223] (1.266 m^2 g^{-1}), Pathak et al. [108] (1.4546 m^2 g^{-1}) and Mendonça et al. [12] (1.0 m^2 g^{-1}) also reported comparatively lower surface areas in their catalysts than that of the present catalyst (CC-500, 27.50 m^2 g^{-1}). Sharma et al. [136] also reported $CaCO_3$ and K_2CO_3 impregnated wood ash catalyst for biodiesel synthesis with the surface areas of 14 and 12 m^2 g^{-1} which are also reasonably lower in terms of surface area and efficiency of the catalyst than that of the present catalyst.

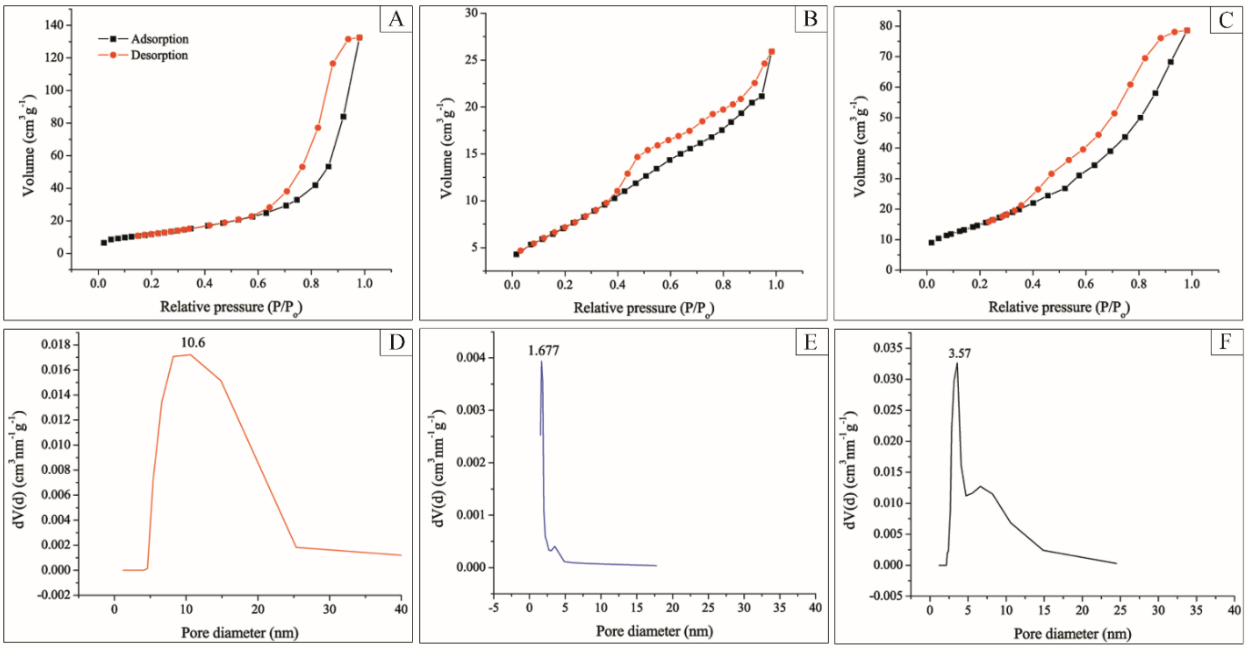

Fig. 2.4. N_2 adsorption-desorption isotherms (A–C) and adsorption pore size distributions (D–F) of *H. fragrans* catalysts calcined at 850 ^{o}C (A, D), 550 ^{o}C (B, E) and burnt ash catalyst (C, F).

2.3.1.4 FESEM analysis

The surface morphological character of the *H. fragrans* catalysts and 3rd recycled catalyst were studied from the FESEM images which are shown in **Fig. 2.5** (A, C, E) and **Fig. 2.6** (A–C), respectively. The FESEM image of the burnt catalyst is demonstrating the cluster of particles and depicting the spongy-like fibrous microstructures. On calcination at 550 and 850

^{o}C, the surface morphology of the catalyst changes to the sheet-like layered structures with non-uniform shapes and sizes and some agglomerated particles are also noticed. The 3rd recycled catalyst of 550 ^{o}C calcined catalyst was also found to be changing slightly in its surface morphology (**Fig. 2.6** A–C) compared to the CC-550 (**Fig. 2.5** C). The appearance of bright particles in the FESEM images might be because of oxygenated materials present in the catalysts which are possibly oxides or carbonates of various metals [113,205,206].

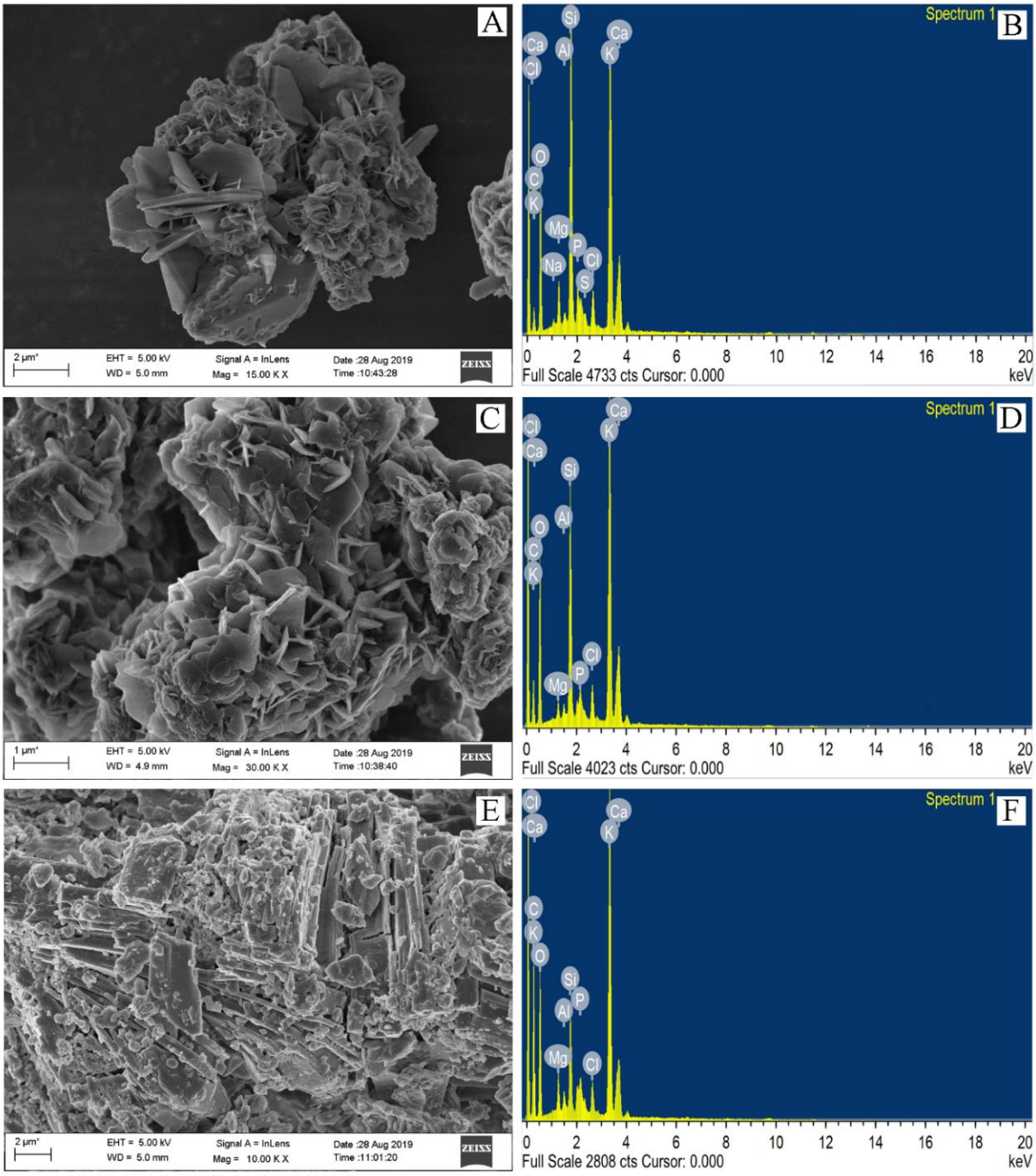

Fig. 2.5. FESEM images (A, C, E) and EDX spectra (B, D, F) of *H. fragrans* catalysts calcined at 850 ^{o}C (A, B), 550 ^{o}C (C, D) and burnt ash catalyst (E, F).

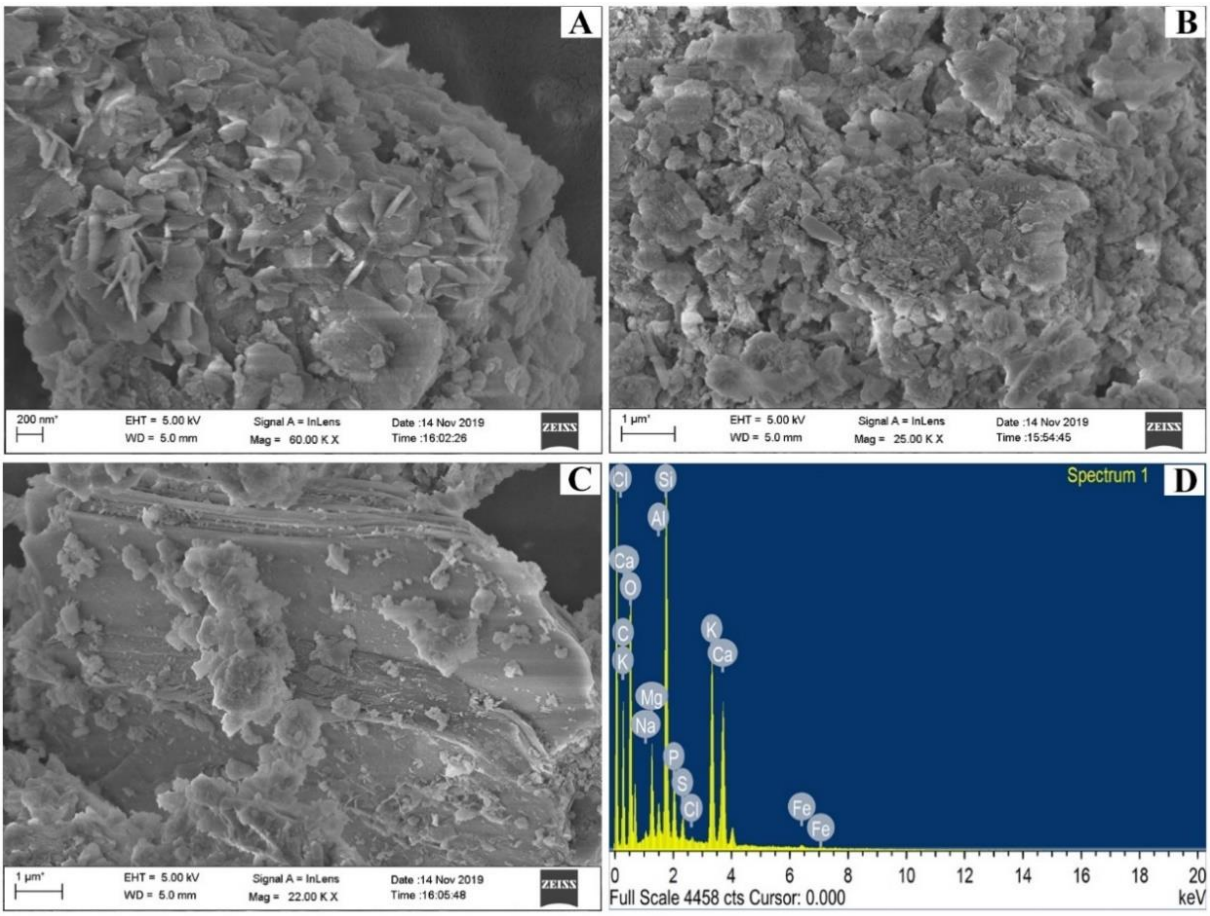

Fig. 2.6. FESEM images (A–C) and EDX spectrum (D) of 3rd recycled of 550 °C calcined *H. fragrans* catalyst.

2.3.1.5 Analysis of elemental composition

EDX spectra of the *H. fragrans* catalysts (**Fig. 2.5** B, D, F) and 3rd recycled catalyst (**Fig. 2.6** D) were recorded to determine the quantitative elemental composition. The results presented in **Table 2.1** indicated the presence of several elements *viz*. C, O, K, Ca, Na, Mg, Al, Si, P, S and Cl. Among the various metals present, potassium concentration was found to be the highest being 14.69 wt.% in BHC, 19.05 wt.% in the CC-550 and 19.27 wt.% in the CC-850. A significantly high percentage of C and O in the catalysts was also noticed (**Table 2.1**) indicating the presence of K_2CO_3 and K_2O which are accountable for the good catalytic efficiency of the catalyst. The K_2CO_3 and K_2O components present in the catalysts were also predicted from XRD analyses (**Fig. 2.2**) and supported by the FT-IR studies as well. However, a significant decrease of carbon content (9.90 wt.%) in the CC-850 from 38.95 wt.% (BHC) and 16.71 wt.% (CC-550) was observed as it was expected. This might be due to decrease of carbonate concentration (K_2CO_3) which is also in support of the XRD results where a very low intense peak of K_2CO_3 was seen in the CC-850 (**Fig. 2.2**, red line) and

accordingly its catalytic activity in biodiesel synthesis was found to be low compared to the CC-550. The heterogeneous base catalyst prepared from agricultural-waste having a high concentration of alkali metals shows efficient catalytic activities in the transesterification process for biodiesel production [12]. Similarly, Betiku et al. [115] in their report on the biobased heterogeneous catalyst for biodiesel production stated that the catalyst with high concentration of potassium shows high efficiency in catalytic activity. Basumatary et al. [129] and Gohain et al. [109] also reported that biomass-derived basic heterogeneous catalyst with high potassium content showed good efficiencies in biodiesel synthesis. A comparative elemental analysis of *H. fragrans* catalyst with other reported agro-wastes ash catalysts is presented in **Table 2.2**. Base catalysts with comparatively less catalytic activities comprising less potassium content than that of the present CC-550 (19.05 %) were reported for the synthesis of biodiesel *viz*. the catalysts reported from *Lemna perpusilla* (11.32 %) [114], *Acacia nilotica* (6.7 %) [136] and camphor tree (1.22 %) [159]. **Table 2.2** reveals that in most of the catalysts containing high potassium contents, the amounts of carbon and oxygen have not been reported and in some catalysts carbon contents were not reported and due to these reasons, the amount of potassium as well as other elements appeared to be high in concentration (%). Such catalysts reported with high potassium contents are *Musa balbisiana* stem (25.09 %) [111], red banana peduncle (42.23 %) [224], *Musa balbisiana* peel (41.37 %) [109], *Musa paradisiacal* peel (54.73 %) [112] and *Carica papaya* stem (56.71 %) [220]. These catalysts were studied in biodiesel synthesis and it was found that some catalysts showed comparable activities and some showed lower catalytic activities in comparison to that of the present *H. fragrans* CC-550. However, the present calcined *H. fragrans* catalyst (CC-550) with 19.05 wt.% of potassium present in the form of K_2O, K_2CO_3 and KCl (**Fig. 2.2**) can efficiently convert *J. curcas* oil to biodiesel and showing the active role of K in the reaction with promising catalytic activity.

Table 2.1: FESEM-EDX analyses of *H. fragrans* catalysts

Elements	**Composition of *H. fragrans* catalysts**							
	Burnt ash		**Calcined at 550 °C**		**3rd recycled of 550 °C calcined catalyst**		**Calcined at 850 °C**	
	Weight %	**Atomic %**	**Weight %**	**Atomic %**	**Weight %**	**Atomic %**	**Weight %**	**Atomic %**
C	38.95	52.22	16.71	25.97	33.84	45.64	9.90	16.58
O	36.37	36.62	46.74	54.54	41.18	41.70	44.75	56.24
K	14.69	6.05	19.05	9.10	6.00	2.48	19.27	9.91
Ca	3.05	1.22	5.13	2.39	5.11	2.07	5.44	2.73
Na	–	–	–	–	0.29	0.21	0.44	0.38
Mg	1.31	0.86	0.86	0.65	2.38	1.59	2.13	1.77
Al	0.50	0.30	0.44	0.31	0.72	0.43	0.40	0.29
Si	2.99	1.71	8.51	5.66	7.91	4.56	12.51	8.95
P	0.80	0.41	0.64	0.38	1.80	0.94	2.27	1.47
S	–	–	–	–	0.64	0.32	0.72	0.45
Cl	1.32	0.60	1.92	1.00	0.13	0.05	2.17	1.23

Surface elemental composition of the *H. fragrans* catalysts determined from XPS studies (**Fig. 2.7**) is shown in **Table 2.3**. The presence of O, C, K, Ca, Si, Sr, Mn, Fe, Zn, Na, Mg and Cl in the catalysts was confirmed from the XPS analyses. The concentration of potassium (atomic %) in XPS analysis was 9.02 % (BHC), 15.19 % (CC-550) and 15.71 % (CC-850) and it was found to be the predominant element among the various metals in XPS studies also and the results were well-supported by the EDX reports of the catalysts (**Table 2.1**). Potassium in *H. fragrans* catalysts was found to be present as K_2O, K_2CO_3 and KCl according to the analysis reports of powder XRD (**Fig. 2.2**) and K_2O and K_2CO_3 were further supported by FT-IR studies (**Fig. 2.3**). In this study, the peaks at binding energies of 530.84 eV (CC-850), 530.88 and 534.84 eV (CC-550) and 531.17 eV (BHC) observed in the XPS spectra of O 1s (**Fig. 2.7** B) are indicating the elemental oxygen of the oxides (metal) present in the catalysts. In the C 1s XPS spectra (**Fig. 2.7** C) of the catalysts, the two peaks one at binding energy of 284.91 eV (BHC, CC-550 and CC-850) and the other at binding energies of 288.73 eV (CC-550) and 289.11 eV (BHC and CC-850) are the indicative of the C=O

carbon (sp^2 hybridized) representing the carbonates of the metals [108]. The deconvolution of XPS spectra of K shown in **Fig. 2.7** D depicted two peaks for all the three catalysts at different binding energies. The characteristic peak (**Fig. 2.7** D) at slightly higher binding energy corresponds to K $2p_{1/2}$ and the other peak at slightly lower binding energy represents K $2p_{3/2}$ designating the potassium (K) in +1 oxidation state. The XPS study may also signify the existence of carbonate (K_2CO_3) and oxide (K_2O) as characterized by XRD (**Fig. 2.2**). It can be stated that the binding energy of potassium in K_2CO_3 is more compared to K_2O, because K–O bond in K_2CO_3 is more ionic with higher polarizability of K compared to K–O bond in K_2O. As we know that the relative covalency of carbon (as C is less basic than K) increases the ionic character of K in K_2CO_3 compared to K in K_2O and accordingly, with increase in ionic character, bond strength increases and concomitantly the binding energy increases [225,226]. In the XPS analysis, the K found in the catalyst calcined at 550 ^oC (CC-550) in the form of K_2CO_3 and K_2O may be represented by the two peaks at binding energies of 295.42 eV and 292.75 eV, respectively. Similarly, the two peaks in the XPS spectra (**Fig. 2.7** D), the first one peak at higher binding energies of 295.25 eV for BHC and 295.42 eV for CC-850 and the other peak with slightly lower binding energies of 292.61 eV for BHC and 292.69 eV for CC-850 may be the indicative of K as K_2CO_3 and/or K_2O. These results are comparable with the reported values in the work of Pathak et al. [108]. In the spectra of Ca 2p (**Fig. 2.7** E), the appearance of the two peaks at binding energies of 345.96 eV (BHC, CC-550 and CC-850) and 349.01 eV (CC-550), 349.94 eV (BHC, CC-850) might be because of the carbonate or oxide of Ca found in the catalysts [50,205]. Silicone due to the presence of SiO_2 in the *H. fragrans* catalysts showed a peak at binding energy of 101.88 eV (BHC), 102.49 eV (CC-550) and 102.29 eV (CC-850) (**Fig. 2.7** F). In this study, the analyses of EDX and XPS revealed the presence of a high amount of potassium which existed as carbonate, oxide and chloride in the *H. fragrans* catalysts (**Fig. 2.2**).

Table 2.2: Elemental composition comparison of *H. fragrans* catalyst with other reported agro-wastes ash catalysts

Ash catalyst	Calcination conditions	Composition (%)													References
		Na	**K**	**Ca**	**Mg**	**Al**	**Si**	**P**	**Cl**	**Fe**	**Mn**	**Zn**	**Sr**	**C**	**O**	
H. fragrans (This work)	550 °C, 2 h	–	19.05	5.13	0.86	0.44	8.51	0.64	1.92	–	–	–	–	16.71	46.74	-
Musa balbisiana underground stem	550 °C, 2 h	0.61 (Na_2O)	25.09 (K_2O)	10.44 (CaO)	10.04 (MgO)	4.07 (Al_2O_3)	35.92 (SiO_2)	4.47 (P_2O_5)	–	1.88 (Fe_2O_3)	–	–	1.89 (SrO)	–	–	[111]
Lemna perpusilla Torrey	550 °C, 2 h	0.53	11.32	–	–	–	82.51	–	1.10	–	–	–	–	5.10	–	[114]
Acacia nilotica tree stem	500 °C	0.6	6.7	13.3	2.7	8.3	15.7	0.80	–	–	–	–	–	–	–	[136]
Musa paradisiacal peels	500 °C, 3.5 h	–	54.73	1.13	-	3.42	33.01	1.99	4.89	0.04	0.05	0.01	0.03	–	-	[112]
Musa balbisiana peels	700 °C, 4 h	10.41	41.37	36.08	12.02	–	–	–	–	–	–	–	–	–	–	[109]
Red banana peduncle	700 °C, 4 h	–	42.23	1.70	1.39	–	1.54	1.91	–	–	–	–	–	–	50.54	[224]

Red banana peduncle	Burnt ash	–	25.63	–	0.97	–	0.56	0.78	–	–	–	–	–	–	72.06	[224]
Carica papaya stem	700 °C, 4 h	14.78	56.71	21.08	4.41	–	3.02	–	–	–	–	–	–	–	–	[220]
Acacia nilotica tree stem	800 °C	5.7	5.7	17.8	4.5	1.2	21.5	0.5	–	–	–	–	–	–	–	[136]
Camphor tree leaf	800 °C, 2 h	0.23	1.22	12.05	1.82	2.70	–	–	–	–	–	–	–	–	–	[159]

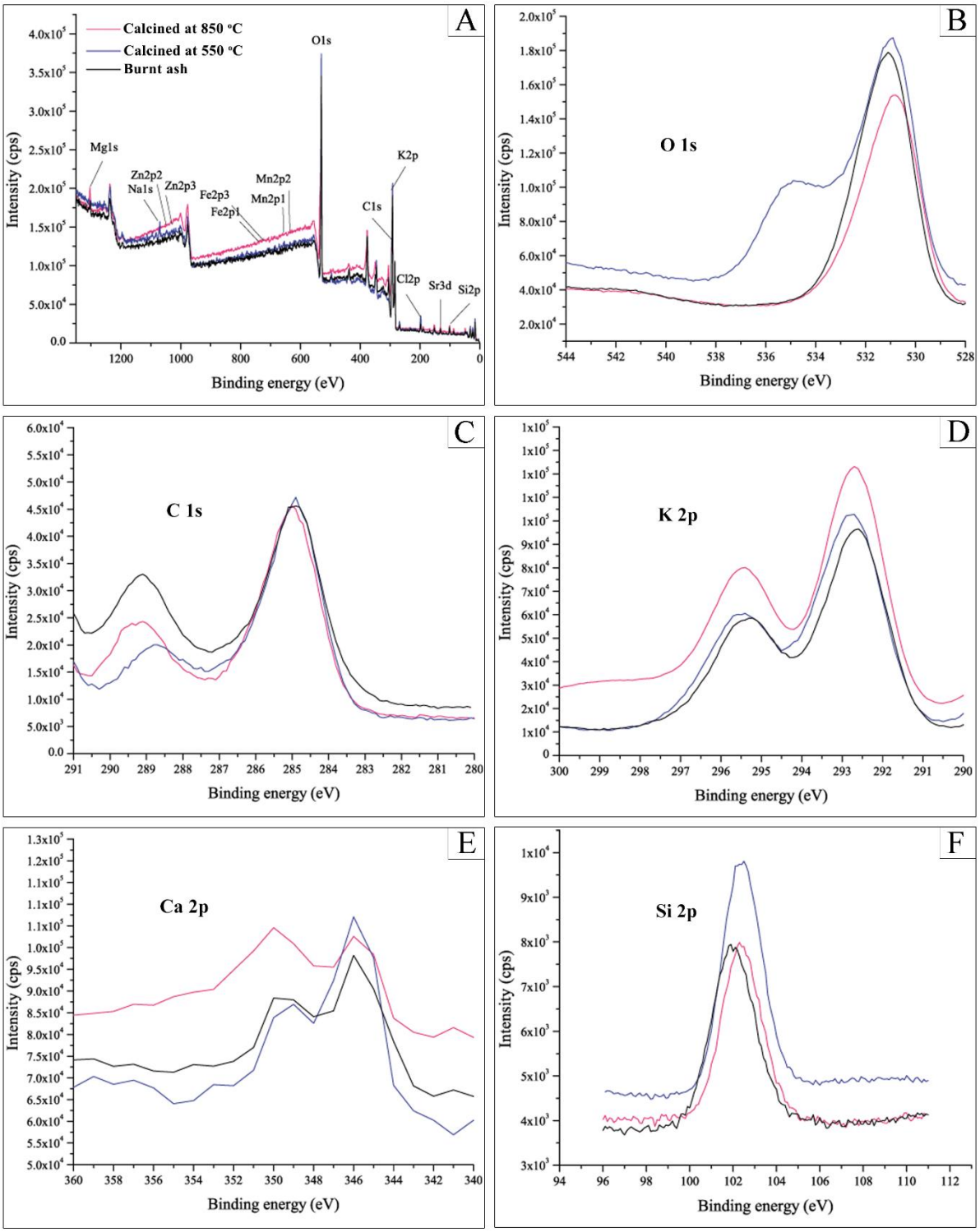

Fig. 2.7. XPS survey spectra (A) of *H. fragrans* catalysts calcined at 850 ºC, 550 ºC and burnt ash catalyst; High resolution XPS spectra of O 1s (B), C 1s (C), K 2p (D), Ca 2p (E) and Si 2p (F).

Table 2.3: XPS analyses of *H. fragrans* catalysts

Elements	**Composition of *H. fragrans* catalysts (Atomic %)**		
	Burnt ash	**Calcined at 550 ºC**	**Calcined at 850 ºC**
C 1s	46.46	36.66	39.59
O 1s	25.12	31.63	23.47
K 2p	9.02	15.19	15.71
Ca 2p	5.15	0.59	5.88
Si 2p	10.59	11.48	11.00
Sr 3d	0.83	0.94	0.78
Mn 2p	0.65	0.55	0.09
Fe 2p	0.29	0.63	0.45
Zn 2p	0.46	0.28	0.46
Na 1s	0.00	0.15	0.63
Mg 1s	0.42	1.21	0.13
Cl 2p	1.01	0.70	1.80

2.3.1.6 HRTEM analysis

HRTEM images of the *H. fragrans* catalysts depicted in **Fig. 2.8** are illustrating the various structural information of the catalysts. It is observed that the burnt *H. fragrans* catalyst (**Fig. 2.8** I, J) is showing the particles with irregular shape and size. When this catalyst is calcined at 550 ^{o}C (**Fig. 2.8** E, F), the particles have acquired needle-like shaped crystals which deforms on further calcination of the catalyst at 850 ^{o}C (**Fig. 2.8** A, B) with the formation of aggregated particles (**Fig. 2.8** A) and some particles of spherical shaped nanostructures (**Fig. 2.8** C). The HRTEM images (5 nm) depicted in **Fig. 2.8** (C, G, K) are showing the fringes of the materials which is the characteristic properties of the mesoporous materials and the mesoporosity of the material is also supported by BET analysis which is shown in **Fig. 2.4**. The SAED patterns of the *H. fragrans* catalysts from HRTEM analysis depicted the polycrystalline nature of the materials (**Fig. 2.8** D, H, L), which is supported by XRD analysis (**Fig. 2.2**) that showed the presence of various inorganic crystalline components. Similarly, SAED patterns with the polycrystalline nature of the basic heterogeneous catalyst was reported from the waste biomass such as *Eichhornia crassipes* in the work of Talukdar and Deka [135]. From the above discussion, it is concluded that the

material is highly porous and crystalline in nature. This type of property is highly important to be a heterogeneous catalyst and it helps to increase the rate of the reaction.

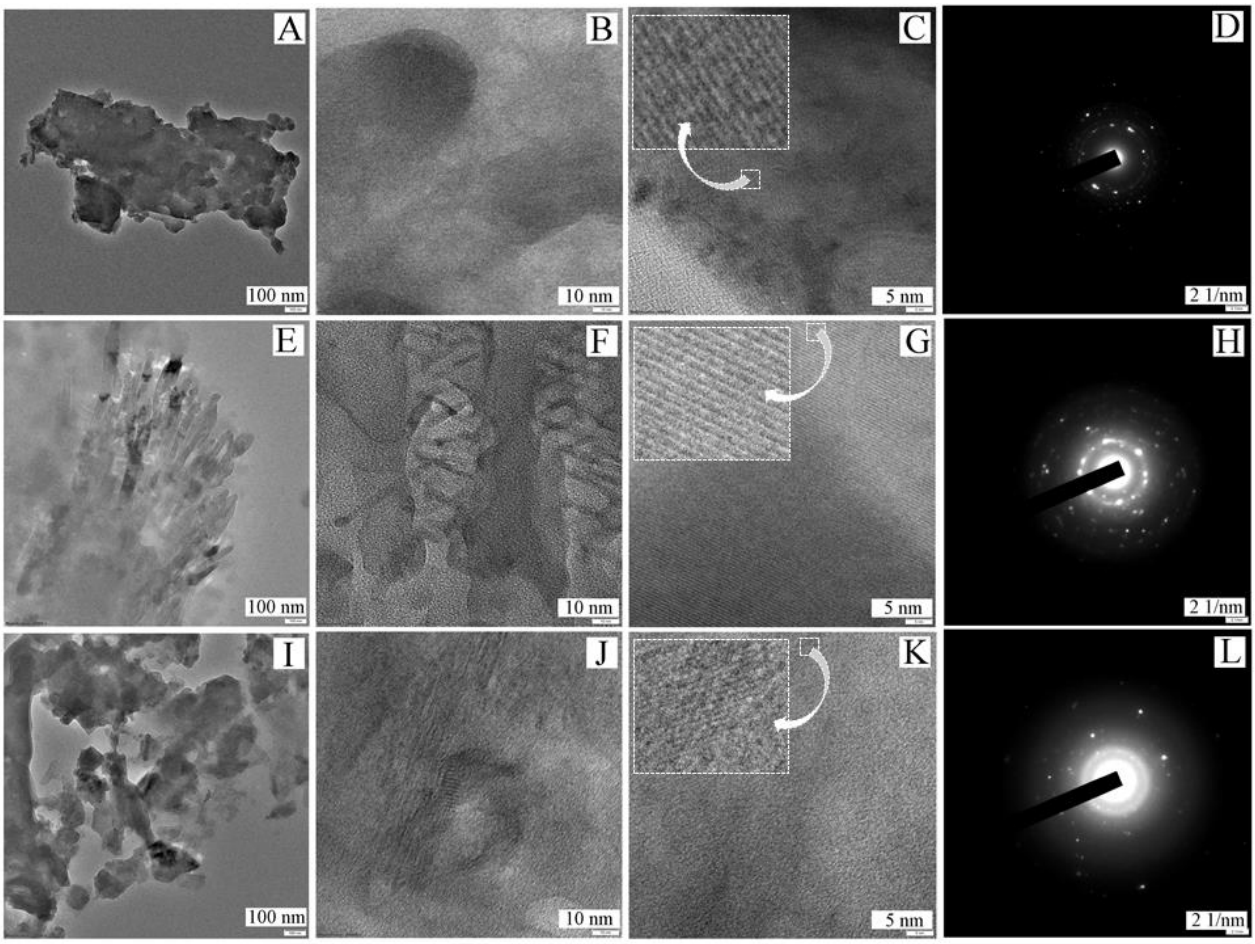

Fig. 2.8. HRTEM images of *H. fragrans* catalysts calcined at 850 ^{o}C (A, B, C), 550 ^{o}C (E, F, G) and burnt ash catalyst (I, J, K) and their respective SAED patterns–D (850 ^{o}C), H (550 ^{o}C) and L (burnt ash catalyst).

2.3.1.7 Measurement of pH value

The determined pH values of the *H. fragrans* catalysts are shown in **Fig. 2.9**. The CC-550 showed the highest pH value of 12.89 at the ratio of 1:5 w/v which decreases to 12.07 at 1:40 w/v. The CC-850 and BHC exhibited the pH value 12.18 and 11.54, respectively at 1:5 w/v which were found to decrease slightly at 1:40 w/v (**Fig. 2.9**, red and black lines). However, the waste-biomass derived base catalyst from *Eichhornia crassipes* (pH = 9.6, 1:20 w/v) [135] displayed lower pH values compared to that of the present catalyst. The high pH value of *H. fragrans* catalyst indicating the high basic nature of the materials could be attributed due to the higher K contents shown in the analysis results of EDX (**Table 2.1**) and

XPS (**Table 2.3**). The K as an active species is found to be present mainly as K_2CO_3 and K_2O (**Fig. 2.2**, **Fig. 2.3**) and it is playing the significant role in the catalysis.

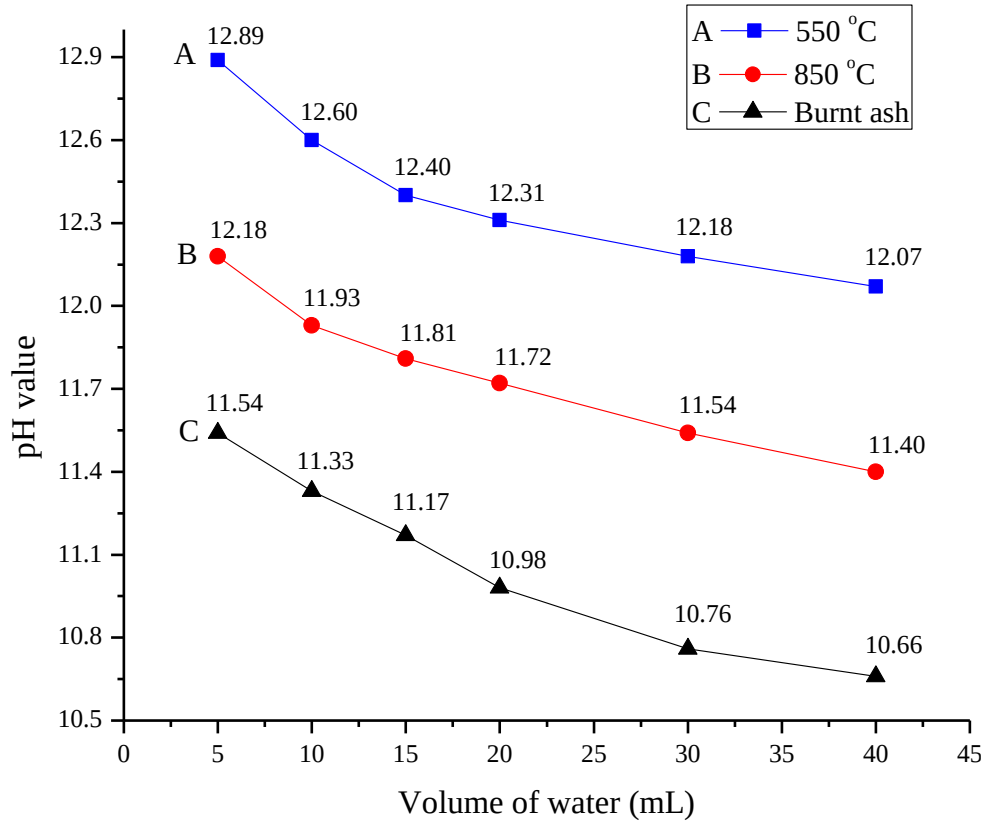

Fig. 2.9. Variation of pH value of *H. fragrans* calcined catalysts (850 °C and 550 °C) and burnt ash catalyst (1 g) with different volume of water.

2.3.1.8 Basicity study of *H. fragrans* catalyst

The basic strength is considered to be the preceding criteria of a catalyst in conducting a base catalysed transesterification and determined employing Hammett method [207]. The determination of basic strength by Hammett indicators shows that all the *H. fragrans* catalysts (BHC, CC-550 and CC-850) are able to change color up to the nile blue ($H_- = 10.1$), however no color change with 4-nitroaniline ($H_- = 18.4$) is observed. The catalyst basic strength is expressed as "stronger than the weakest indicator that exhibits a color change, but weaker than the strongest indicator that exhibits no color change" [227,228]. Thus, the basic strength of all the catalysts is found to be in the range of $10.1 < H_- < 18.4$. The catalyst CC-550 displayed the highest basicity of 0.423 mmol/g followed by the catalyst CC-850 of 0.303 mmol/g and the burnt catalyst (BHC) of 0.298 mmol/g and this trend is matching with the pH studies of the catalysts (**Fig. 2.9**). In accordance with the highest

basicity, the CC-550 exhibited the better catalytic efficiency in converting the jatropha oil to biodiesel compared to CC-850 and BHC, which showed quite comparable basicity with almost analogous catalytic results (**Fig. 2.10**). Turnover frequency (TOF), number of moles of the produced biodiesel molecule per unit basic active site and per time, which indicates the catalytic efficiency of the heterogeneous catalyst was calculated following the equation (2.4) [207] and found to be 35.55 min^{-1}, 27.71 min^{-1} and 29.47 min^{-1} for CC-550, CC-850 and BHC, respectively.

$$\text{Turnover frequency (TOF)} = \frac{\text{Moles of produced biodiesel}}{\text{Basicity} \times 0.001\ (\text{mol}) \times \text{time}} \qquad (2.4)$$

2.3.2 Catalytic activity of the *Heteropanax fragrans* catalyst

2.3.2.1 Effect of calcination temperature of the prepared catalyst

To study the effect of calcination temperatures on the catalytic efficiency of *H. fragrans* catalyst, the BHC, CC-550 and CC-850 were utilized in transesterification of *J. curcas* oil at the ORCs of MTOR of 12:1 and catalyst dose of 7 wt.% at 65 ^oC. The results of the investigation shown in **Fig. 2.10** indicated that the *H. fragrans* CC-550 is exhibiting better performance with a high biodiesel yield of 97.75 % in 65 min compared to the BHC (96.61 %, 110 min) and the CC-850 (96.58 %, 115 min). The basicity of burnt catalyst starts increasing from 0.298 to 0.423 mmol/g when it is calcined at 550 ^oC, whereas increasing the calcination temperature till 850 ^oC, the basicity falls to 0.303 mmol/g. The burnt catalyst becomes more active for the reaction when it is activated at 550 ^oC, however, the catalytic activity is found to decrease when it is further calcined at 850 ^oC. Thus, the high catalytic activity could be explained on the basis of higher basicity measured through Hammett method. With increase in the calcination temperature up to 850 ^oC, the carbonate concentration of metals in the catalyst may decrease and accordingly, activity for the reaction decreases. It is remarkable to mention from XRD analysis that the high intense peak due to K_2CO_3 at 2θ value of 26.68 in the BHC and at 2θ value of 26.65 in the CC-550 decreases in the XRD pattern (**Fig. 2.2**, red line) of the CC-850 (2θ = 26.68). This might be because of the decrease of carbonate (CO_3^{2-}) concentration (K_2CO_3) in the catalyst on increasing the calcination temperature to 850 ^oC which may be due to the partial conversion or decomposition of K_2CO_3 to K_2O at the higher temperature (850 ^oC). In FI-IR spectra (**Fig. 2.3**) of catalysts, it is also observed that the peaks due to carbonates (K_2CO_3) are gradually transformed and decreased (at 1639, 1465, 1416 and 1384 cm^{-1}) with increase in calcination

temperature (**Fig. 2.3**, red line) which is in agreement with XRD analysis (**Fig. 2.2**). K_2CO_3 due to its weak acid and strong base is more basic than K_2O and hence, the CC-550 may be due to its high concentration of K_2CO_3 is found to be better in catalytic activity followed by the BHC and the CC-850. In agreement with the predicted XRD and FT-IR results, the decrease in the amount of carbonate at higher calcination temperature (CC-850) decreases the basic character which is confirmed by its lower pH value of 12.18 at 1:5 w/v compared to the CC-550 with the highest pH value of 12.89 at 1:5 w/v. The lower efficiency in the transesterification reaction of the BHC might be because of the presence of its more carbonaceous matter revealed from the results of EDX (C = 38.95 %, **Table 2.1**) and XPS (C = 46.46 %, **Table 2.3**) analyses and also due to its lower pH value (11.54 at 1:5 w/v) compared to the activated CC-550 which is having lower carbon contents of 16.71 % (EDX) and 36.66 % (XPS) and higher pH value (12.89 at 1:5 w/v). Thus, the CC-550 is found to be superior which displayed better results yielding 97.75 % of *J. curcas* biodiesel in 65 min at MTOR of 12:1, catalyst dose of 7 wt.% and 65 ^oC. Similarly, Chouhan and Sarma [114] and Sarma et al. [111] also successfully utilized biomass-based catalysts calcined at 550 ^oC in biodiesel production.

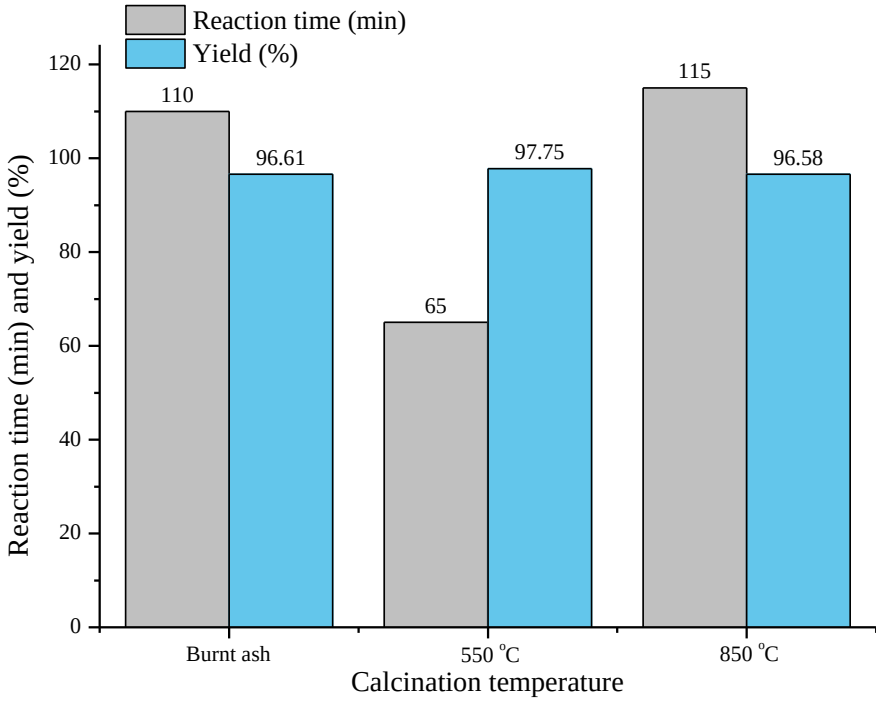

Fig. 2.10. Effect of catalyst calcination temperatures (850 ^oC, 550 ^oC and burnt ash) of catalyst on J. curcas biodiesel production via transesterification (Reaction temperature = 65 ^oC, MTOR = 12:1, catalyst loading = 7 wt.%).

2.3.2.2 Effect of catalyst dosage

Catalyst dosage has varied influences on the rate of oil transesterification as well as on the yield of produced biodiesel. Hence, in this study, *J. curcas* biodiesel production was investigated using the *H. fragrans* catalyst calcined at 550 ^{o}C (CC-550) by varying the catalyst loading (3, 5, 7 and 9 wt.% of oil) with 12:1 MTOR at 65 ^{o}C (**Fig. 2.11**). The results reveal that on increasing the amount of the catalyst from 3 to 7 wt.%, the reaction time was found to decrease significantly from 185 min to 65 min with a significant increase in the yield of *J. curcas* biodiesel from 91.96 to 97.75 %. It is also noticed that further increase of catalyst dose to 9 wt.% does not noticeably decrease the reaction time (55 min) and significant increase in the yield of biodiesel (97.40 %) was also not achieved which is in accordance with the perception that the increase of catalyst dosage beyond the optimum concentration does not enhance the yield of biodiesel [109]. Hence, the 7 wt.% of catalyst concentration is considered as the optimum reaction condition for *H. fragrans* catalyst in transesterification of *J. curcas* oil to its biodiesel. The rice husk ash catalyst was also reported by Chen et al. [229] with 7 wt.% as the optimum catalyst dose for their reaction of palm oil to biodiesel.

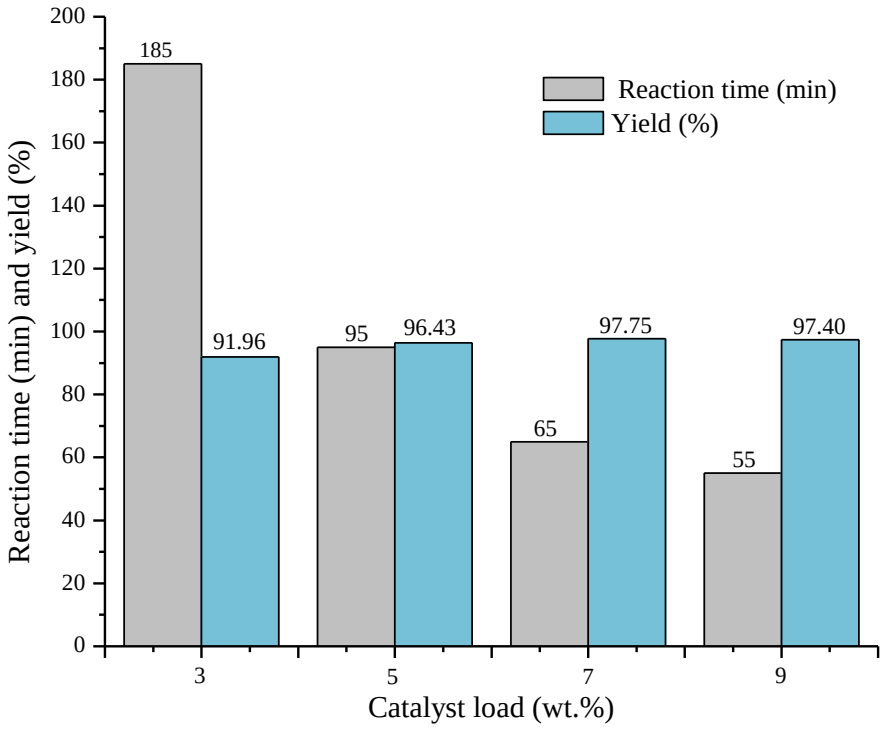

Fig. 2.11. Effect of *H. fragrans* calcined catalyst (550 ^{o}C) loading on *J. curcas* biodiesel production (MTOR = 12:1, temperature = 65 ^{o}C).

2.3.2.3 Effect of MTOR (methanol to oil ratio)

MTOR similar to that of catalyst concentration has influences on the rate of reaction and product yield of biodiesel synthesis. Hence, the investigation on the reaction was carried out by varying the MTOR using the optimized amount of catalyst (7 wt.%, CC-550) at 65 ^{o}C (**Fig. 2.12**). When MTOR is increased from 3:1 to 12:1, a significant increase in the yield of *J. curcas* biodiesel from 89.45 to 97.75 % along with the considerable decrease in the reaction time from 185 to 65 min was observed (**Fig. 2.12**). Further increase in MTOR to 15:1 results no decrease in reaction time without any further increase in biodiesel yield (97.21 %), whereas a gradual increase in reaction time (75 min) is observed when 18:1 MTOR was used with no significant improvement in the yield of biodiesel (97.43 %). A similar trend of the experimental result was also reported in the work of Syazwani et al. [230] and in their report, it was stated that higher levels of MTOR beyond optimum reaction condition dilute the reaction mixtures resulting to the flooding of catalyst's active sites which in turn decreases their interactions for efficient reaction and as a result, the rate of reaction and the product (biodiesel) yield decrease. Moreover, beyond the optimum MTOR level, there is always a chance which may increase the hydrolysis of produced biodiesel (esters of methyl) to form soap and this will cause to the reduced yield of biodiesel [222]. In the present investigation, the optimum level for *J. curcas* oil transesterification to biodiesel was found to be 12:1 of MTOR with 7 wt.% of CC-550. For biodiesel synthesis via transesterification, a similar optimum MTOR level of 12:1 was also reported by Taslim et al. [231] with corncob ash catalyst, Sharma et al. [136] and Uprety et al. [171] with wood ash catalyst and Wang et al. [223] with gasified straw slag catalyst.

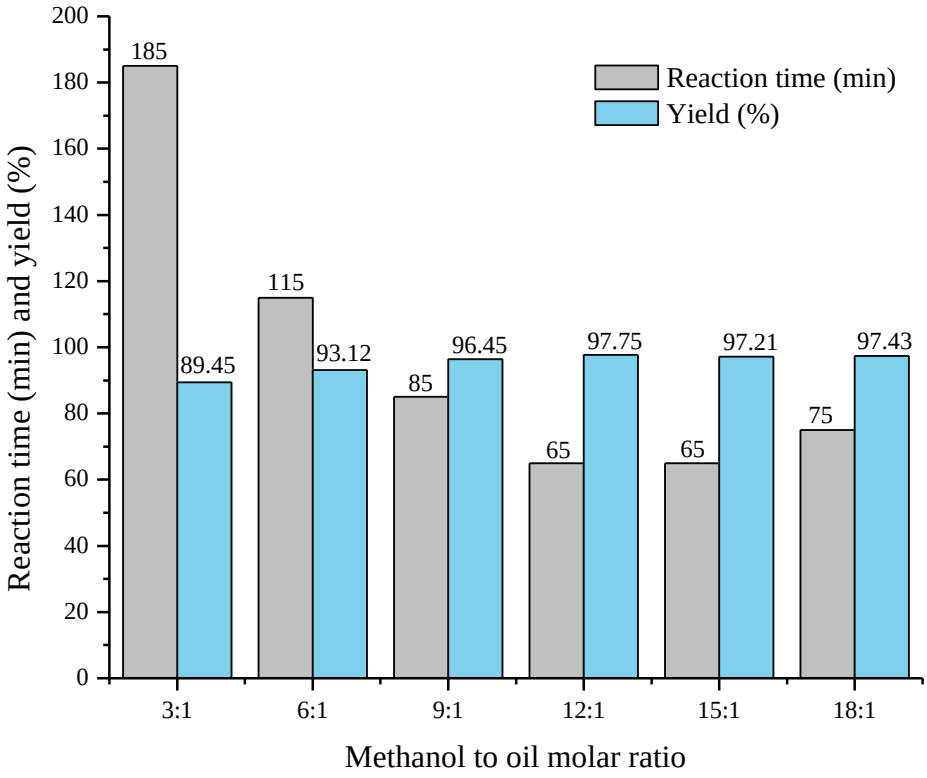

Fig. 2.12. Effect of MTOR on *J. curcas* biodiesel production via transesterification (Reaction temperature = 65 ^{o}C, loading of catalyst calcined at 550 ^{o}C = 7 wt.%).

2.3.2.4 Effect of reaction temperature

In this study, the transesterification of *J. curcas* oil for biodiesel production was carried out at various reaction temperatures using ORCs of MTOR (12:1) and catalyst (7 wt.% of CC-550) and the results are shown in **Fig. 2.13**. The results revealed that when the temperature is raised from 32 to 65 ^{o}C, there is a significant reduction in the time period of the reaction from 205 to 65 min with comparable *J. curcas* biodiesel yield (97.63 % and 97.75 %). On further increase of temperature to 75 ^{o}C, no significant change or decrease in reaction time (60 min) is noticed and at the same time, the yield of biodiesel from *J. curcas* oil also remains unchanged (**Fig. 2.13**). Thus, the better performance of the reaction was found to be at 65 ^{o}C with 12:1 MTOR and 7 wt.% of catalyst yielding 97.75 % biodiesel and therefore, 65 ^{o}C is taken as the optimum reaction temperature for the present study. Similar results (65 ^{o}C) with the utilization of biomass-based heterogeneous catalysts in biodiesel syntheses were also reported by Adesina et al. [232], Odude et al. [106], Chouhan and Sarma [114] and Sharma et al. [136].

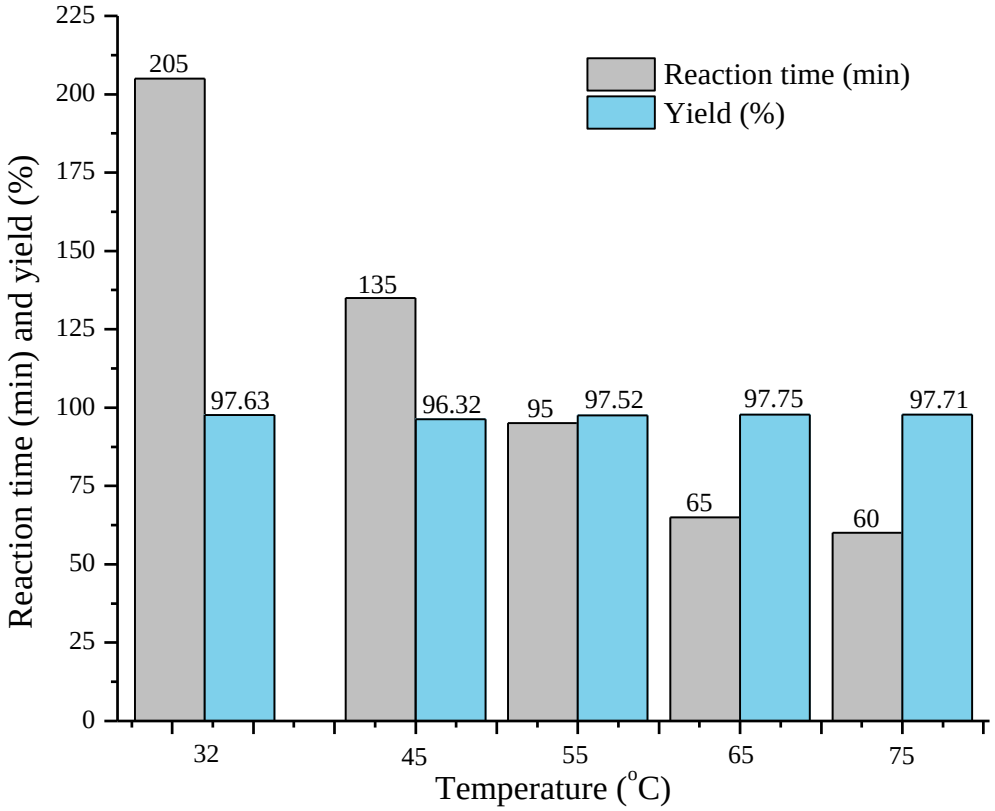

Fig. 2.13. Effect of reaction temperatures (32, 45, 55, 65 and 75 ^{o}C) on *J. curcas* biodiesel production via transesterification (MTOR = 12:1, Loading of catalyst calcined at 550 ^{o}C = 7 wt.%).

2.3.2.5 Determination of activation energy and pre-exponential factor

To study activation energy (Ea) and frequency factor (A) of the transesterification of *J. curcas* oil using *H. fragrans* catalyst calcined at 550 ^{o}C (CC-550), we performed the reactions at 32, 45, 55, 65 and 75 ^{o}C and calculated the value of the rate constant (k) [205] and found to be 0.02, 0.02, 0.04, 0.06 and 0.06 min^{-1}, respectively. Thereafter, the activation energy (Ea) and the frequency factor (A) were calculated from the *straight-line slope (Slope = - Ea/R; R* = 8.314 J K^{-1} mol^{-1}) and intercept (Intercept = ln A), respectively obtained from the Arrhenius plot (**Fig. 2.14**). The value of the slope of the straight line was found to be -3.8868 and therefore, the Ea of the reaction was determined as 32.31 kJ mol^{-1}. Accordingly, the intercept (ln A) of the straight line was found to be 7.06276 and the value of frequency factor was 1.155 × 10^{7} min^{-1}. However, the relatively higher Ea of 61.23 kJ mol^{-1} was reported by Mendonça and Co-worker [12] for tucumã peel ash catalysed biodiesel production from soybean oil in comparison to the *H. fragrans* catalysed reaction demonstrating the more efficacy of the present catalyst. The activation energy for the

production of biodiesel through transesterification of oil has been reported to be within *21–84 kJ mol*$^{-1}$ and the value of the present study is well within this range [205,211,212]. It has been found that the diffusion-controlled reactions have the Ea values within 10–15 kJ mol^{-1} and the chemically-controlled reactions have Ea values of more than 25 kJ mol^{-1} and accordingly, the *H. fragrans* (CC-550) catalysed biodiesel synthesis from *J. curcas* oil is indicating the chemically controlled reaction [205,212].

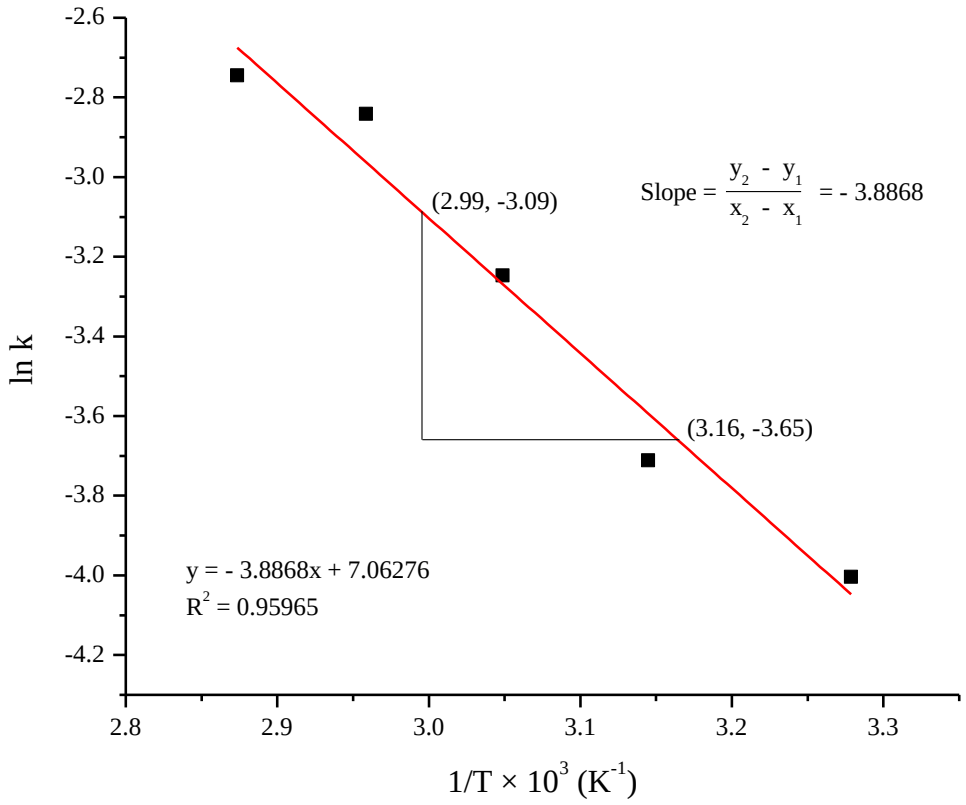

Fig. 2.14. Arrhenius plot of ln k vs 1/T for *H. fragrans* catalysed transesterification of *J. curcas* oil to biodiesel.

2.3.3 Comparative study of *Heteropanax fragrans* catalyst with other reported basic heterogeneous catalysts

The investigation on the effects of catalyst loading, MTOR, reaction temperature and calcination temperature of the *H. fragrans* catalyst on transesterification of *J. curcas* oil disclosed the maximum biodiesel yield of 97.75 % in a reaction time of 65 min under the ORCs of MTOR of 12:1 and 7 wt.% of catalyst loading (CC-550) at the reaction temperature of 65 ^{o}C. The results are compared with the already reported waste biomass-based basic heterogeneous catalysts that were used for biodiesel production and shown in **Table 2.4**. In the synthesis of biodiesel using the solid base catalysts, Sarma et al. [111], Aslam et al. [110]

and Kumar et al. [197] reported very high reaction temperatures (275 and 200 ^{o}C) for transesterification with approximately similar biodiesel yields indicating the lower efficacy of the catalyst compared to the catalyst of the present work (**Table 2.4**). In several studies of biodiesel production using various waste-based heterogeneous base catalysts, Mendonça et al. [12], Deka and Basumatary [11], Wang et al. [223], Pathak et al. [108], Chouhan and Sarma [114], Gohain et al. [109] and Sharma et al. [136] reported lower catalytic activities with longer reaction times which may be due to significantly lower surface areas of these catalysts compared to the present *H. fragrans* catalyst having the larger surface area of 27.50 $m^2 g^{-1}$ (**Table 2.4**). Betiku et al. [105] reported comparable catalytic activity for biodiesel production with banana peel ash catalyst having a low surface area of 4.442 $m^2 g^{-1}$. The *H. fragrans* catalyst is far better in its activity for biodiesel production compared to the Birch bark ash catalyst [171]. Similarly, the present CC-550 is showing superior catalytic activity for biodiesel production than even the K_2CO_3 loaded camphor tree ash catalyst [159]. *Lemna perpusilla* Torrey ash [114], *Acacia nilotica* stem ash [136] and camphor tree leaf ash [159] exhibited lower catalytic activities in biodiesel production due to the presence of low amounts of potassium in these catalysts compared to present *H. fragrans* catalyst which is having a higher potassium content of 19.05 wt.%. In this study, EDX and XPS analyses revealed the presence of a high amount of potassium in the *H. fragrans* catalysts in comparison to other metals (**Table 2.1**, **Table 2.3**) and the K as an active species in the form of K_2CO_3 and K_2O played the major role in the catalysis for biodiesel production. Thus, the biobased *H. fragrans* catalyst is considered a potential catalyst for low-cost and environmentally friendly production of biodiesel.

Table 2.4: Activity comparison of *H. fragrans* derived base catalyst in biodiesel synthesis with other reported agro-wastes ash catalysts

Biodiesel feedstock	**Catalyst source (Ash)**	**Surface area ($m^2 g^{-1}$)**	**Parameters**				**Biodiesel, Y or C (%)**	**References**
			MTOR	**Catalyst (wt.%)**	**Temp (°C)**	**Time (min)**		
Jatropha oil	*H. fragrans*	27.50	12:1	7	65	65	97.75 (Y)	This work
Jatropha oil	MBUS	38.71	9:1	5	275	60	98 (Y)	[111]
Mesua ferrea oil	MBUS	38.71	9:1	5	275	60	95 (C)	[110]
Jatropha oil	SrO-MBUS	0.043	9:1	5	200	60	96 (Y)	[197]
Palm oil	Banana peel	-	3:2.4	4	65	65	99.5 (Y)	[106]
Soybean oil	Tucumã peels	1.0	15:1	1	80	240	97.3 (C)	[12]
Thevetia peruviana oil	*Musa balbisiana* trunk	1.487	20:1	20	32	180	96 (Y)	[11]
Rapeseed oil	Gasified straw slag	1.266	12:1	20	200	480	95 (C)	[223]
Soybean oil	*Musa acuminata* peel	1.4546	6:1	0.7	32	240	98.95 (C)	[108]
Jatropha oil	*Lemna perpusilla*	9.622	9:1	5	65	300	89.43 (Y)	[114]
Waste cooking oil	*Musa balbisiana* peel	10.176	6:1	2	60	180	100 (C)	[109]
Jatropha oil	$CaCO_3$-Wood ash	14.0	12:1	5	65	180	91.7 (C)	[136]
Jatropha oil	K_2CO_3-Wood ash	12.0	12:1	5	65	180	99 (C)	[136]
Jatropha oil	*Acacia nilotica* stem	3.72	12:1	5	65	180	98.7 (C)	[136]
Palm oil	Birch bark	–	12:1	3	60	180	69.7 (C)	[171]
Soybean oil	K_2CO_3-Camphor tree ash	–	14:1	5	65	210	92.27 (Y)	[159]

MTOR–methanol to oil ratio; wt–weight; min–minute; Temp–temperature; C–conversion; Y–yield; MBUS–*Musa balbisiana* underground stem.

2.3.4 Reusability study of *H. fragrans* catalyst

One of the major advantages and beneficial properties of the solid catalysts is that they can be profitably reused in the consecutive reaction cycles for low-cost production of biodiesel [12, 206, 229]. The reusability of the reaction was investigated using the best *H. fragrans* catalyst (CC-550) following the ORCs (7 wt.% catalyst, 12:1 MTOR and 65 ^{o}C). The catalyst was recovered from the first run of the reaction through filtration followed by washing with hexane for 4–5 times and then with acetone for 2 times to completely remove the products (methyl esters) and glycerol from the catalyst. Thereafter, the catalyst was allowed to dry in the oven at 110 ^{o}C for 4 h, cooled and reused in the transesterification reaction and for every reaction cycle, a similar process was maintained to recover the catalyst. The reusability results (**Fig. 2.15**) indicated that *H. fragrans* catalyst can be effectively recycled up to the 3rd cycle of transesterification reaction with a gradual decrease in the efficacy of the catalyst from 97.75 % (fresh catalyst, 65 min) to 90.22 % (3rd cycle, 215 min). It has been reported that the presence of potassium as an active component in the biomass-based catalyst plays an important role in the catalytic activities for biodiesel synthesis and accordingly, the decrease of this component leads to reduced catalytic activity [206]. The recovered catalyst from the 3rd reaction cycle was characterized by FESEM (**Fig. 2.6** A–C), EDX (**Fig. 2.6** D) and FT-IR (**Fig. 2.3**, green line). The elemental study of the 3rd recycled catalyst (**Table 2.1**) showed a significant decrease of potassium content from 19.05 wt.% (fresh catalyst) to 6.00 wt.% (3rd recycled catalyst), which confirms the loss or leaching of active potassium component during catalyst recycling processes and as result of this, the efficiency of the catalyst in biodiesel production is decreased. Further, the FESEM images of the 3rd recycled catalyst (**Fig. 2.6** A–C) depicted some changes of morphological characters on its reuse and accumulation of particles on the surface of the catalyst which may be due to glycerol molecule (**Fig. 2.3**, green line, 2926 and 2854 cm $^{-1}$ may be due to C-H stretching of glycerol backbone) leading to a coating on the active sites of the catalyst on repeated use, which ultimately leads to decrease in activity of the catalyst. Similarly, in the FI-IR spectrum also (**Fig. 2.3**, green line), some changes of the absorption peaks were observed which may be due to changes in the physical or chemical properties of the materials during catalyst recycling. Similarly, Pathak et al. [108] also mentioned the accumulation of glycerol molecule on the catalyst's surface which blocks the active sites of the catalyst during the process of catalyst recycling leading to reduced efficacy of the catalyst. Pathak et al. [108], Deka and Basumatary [11] and Chouhan and Sarma [114] also reported a gradual decrease in the efficiencies of their catalysts for biodiesel production during reusability studies.

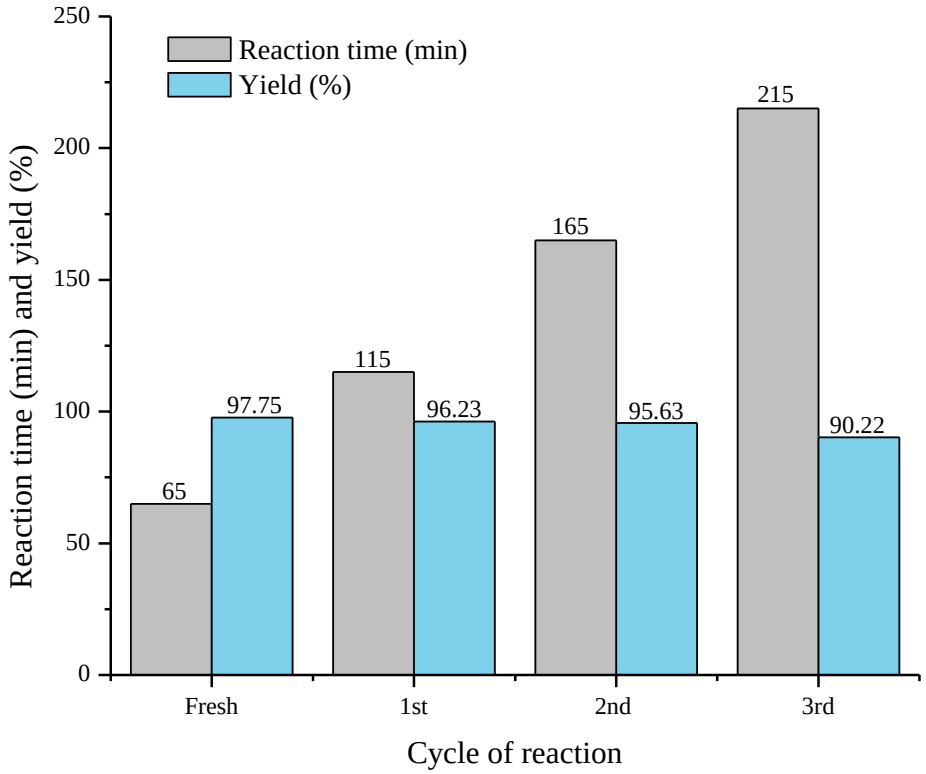

Fig. 2.15. Reusability study of *H. fragrans* catalyst calcined at 550 ^{o}C on *J. curcas* biodiesel production (Reaction temperature = 65 ^{o}C, MTOR = 12:1, Catalyst loading = 7 wt.%).

2.3.5 Mechanism of transesterification catalysed by *H. fragrans* derived solid base catalyst

In this study, the solid heterogeneous base catalyst derived from *H. fragrans* (**Scheme 2.1**) predominantly contains K in the form of K_2CO_3 and K_2O and the reaction is considered as a base catalysed transesterification (**Scheme 2.2**). It is known that in the base catalysed transesterification with methanol, the nucleophilic methoxide ion is produced through the interaction between the active species of the catalyst and methanol. However, in the recent studies of biodiesel production using solid base catalysts *viz*. K modified ceria oxide and $BaSnO_3$, Roy and Co-worker [207,233] stated that methoxide of potassium or barium was not spotted, but they represented more feasible interaction between the triacylglycerol molecule and K–O or Ba–O bond which follows the Eley-Rideal mechanism. On the basis of this idea, the proposed plausible mechanism of the present study with the solid catalyst is depicted in **Scheme 2.2**. Firstly, the basic active species K–O (K_2CO_3 and K_2O) interacts with the triacylglycerol and the molecule is adsorbed at the active surface of the catalyst. The methanol then interacts with the adsorbed triacylglycerol molecule following the mode of

nucleophilic reaction and methyl esters (biodiesel) are formed, which is expected to be released rapidly from the surface of the catalyst. In the third step, insertion of H–atom to the backbone of adsorbed glycerol moiety takes place and desorbs the by-product glycerol molecule from the surface of the catalyst. The active site of the catalyst is regenerated for further interaction with the triacylglycerol molecule.

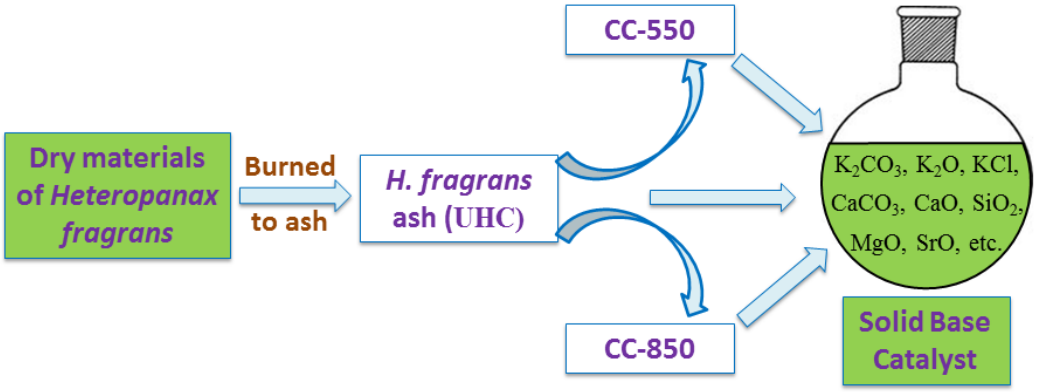

Scheme 2.1. Solid base catalyst derived from *H. fragrans* utilized in biodiesel synthesis.

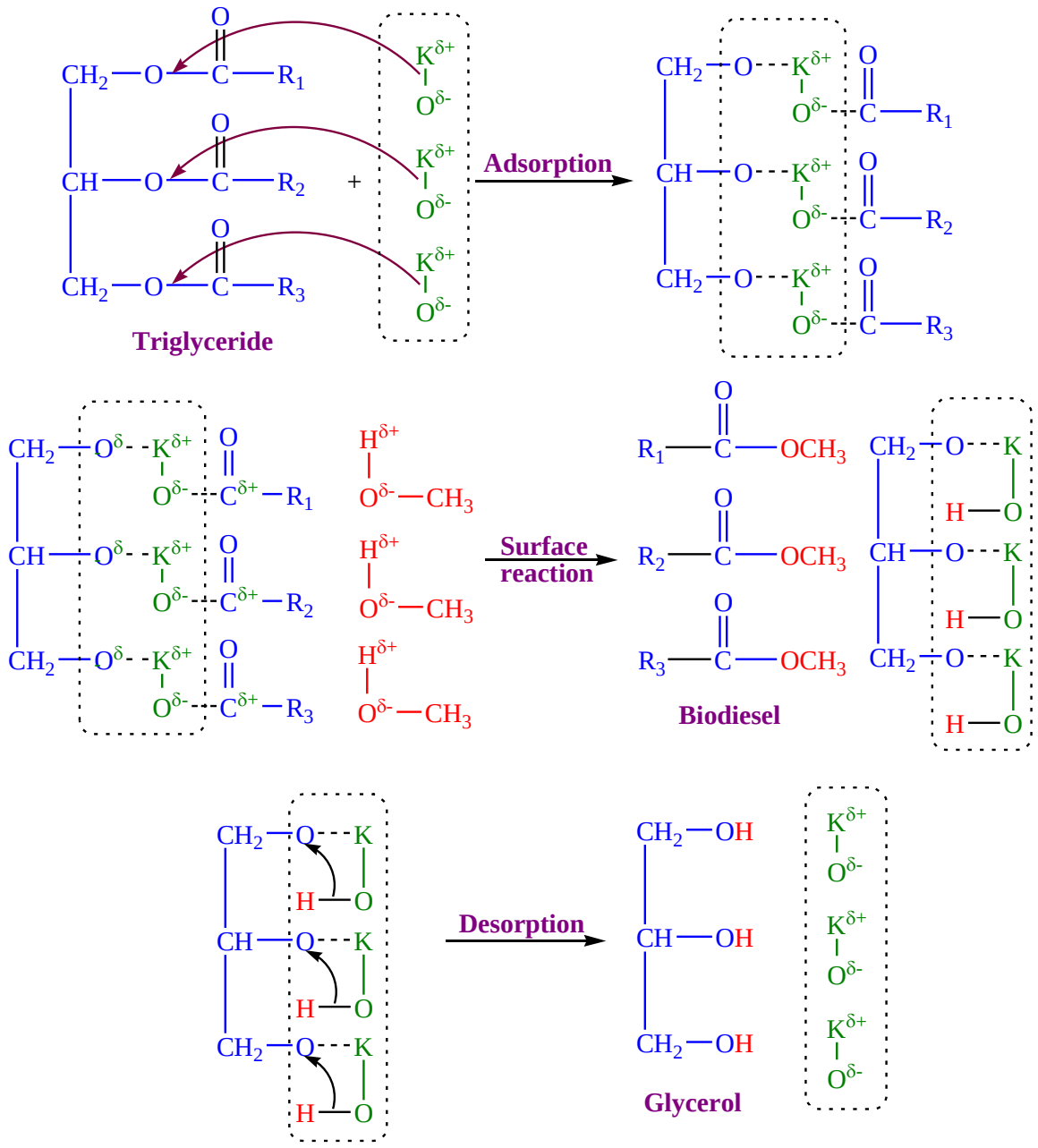

Scheme 2.2: Heterogeneous Solid Base Catalysed Transesterification of vegetable oil to biodiesel (FAME) [234].

2.3.6 Analysis of *J. curcas* biodiesel

2.3.6.1 FT-IR analysis

FT-IR spectra of *J. curcas* oil and biodiesel are depicted in **Fig. 2.16**. The stretching vibration due to carbonyl (C=O) groups of the triglyceride showed a peak at 1746 cm^{-1} which changes to 1742 cm^{-1} in the spectrum of *J. curcas* biodiesel due to C=O stretching vibrations of methyl esters (RCOOMe) indicating the conversion of triglyceride to biodiesel (**Fig. 2.16**). The peaks due to stretching frequencies of =C–H (alkene) in the fatty acid chains of the

triglyceride (oil) and biodiesel exhibited peaks at 3013 and 3007 cm^{-1}, respectively. Accordingly, the peaks representing the C–H stretching vibrations were observed at 2932, 2913 and 2853 cm^{-1} in the oil and at 2926 and 2854 cm^{-1} in the biodiesel. Peaks at 1465 and 1380 cm^{-1} in the oil and at 1454, 1429 and 1361 cm^{-1} in the biodiesel depicted the bending vibrations of terminal CH_3 [205,206]. The peaks due to C–O stretching vibrations of the triglyceride appeared at 1163, 1144 and 1099 cm^{-1} and that of methyl ester molecules of biodiesel appeared at 1192 and 1163 cm^{-1}. The signal at 733 and 724 cm^{-1} in the oil and biodiesel, respectively are representing the -CH_2- rocking of the long chains.

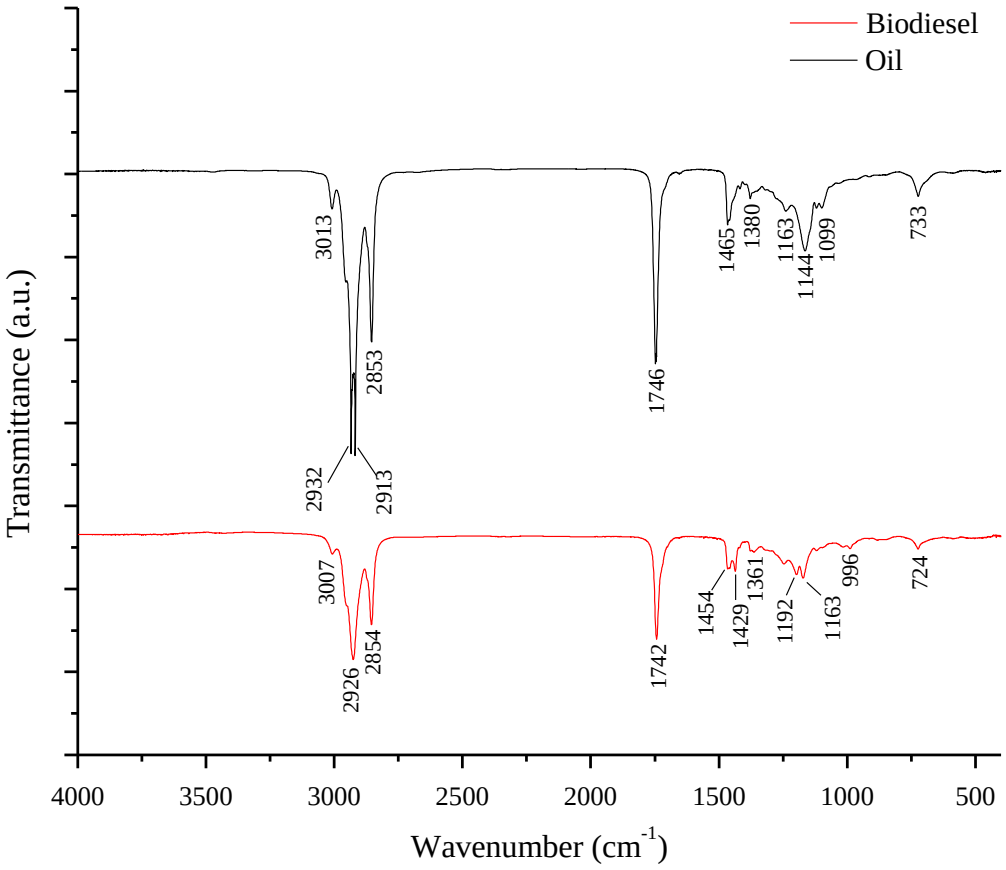

Fig. 2.16. FT-IR spectra of *J. curcas* oil and biodiesel synthesised by *H. fragrans* catalyst.

2.3.6.2 NMR analysis

J. curcas oil and its biodiesel were characterized by ^{1}H NMR spectra (**Fig. 2.17**) and ^{13}C NMR spectra (**Fig. 2.18**). Different types of protons and carbons found in *J. curcas* oil and biodiesel were interpreted and shown in **Table 2.5**. It is observed from the **Table 2.5** that the methine proton signal at δ 5.280 ppm due to C2 in the triglyceride of *J. curcas* oil (-C***H***-CO_2R) and methylene protons signals at *δ* 4.116–4.324 ppm due to C1 and C3 in the triglyceride of *J. curcas* oil (-C***H***$_2$-CO_2R) ***(Fig. 2.17 A)*** are disappearing completely in the *^{1}H*

NMR spectrum of J. curcas biodiesel (**Fig. 2.17** B) with the appearance of a one new singlet signal at δ 3.657 ppm because of the methoxy protons (-CO-OC***H***$_3$), which is showing the conversion of *J. curcas* oil to its biodiesel. Likewise, the methine carbon signal at δ 68.955 ppm due to C2 in the triglyceride (-***C***H-CO_2R) and the signal of methylene carbons at δ 62.091 ppm due to C1 and C3 in the triglyceride of *J. curcas* oil (-***C***H_2-CO_2R) in ^{13}C NMR spectrum ***(Fig. 2.18** A) are* disappearing in the ^{13}C NMR spectrum of *J. curcas* biodiesel (**Fig. 2.18** B) with the appearance of a new signal for the methoxy carbons (-CO-O***C***H_3) of biodiesel at δ 51.423 ppm confirming the transformation of *J. curcas* oil (triglycerides) to biodiesel.

Table 2.5: NMR spectra analyses of *J. curcas* oil and biodiesel synthesised by *H. fragrans* catalyst

Types of protons/carbons	**Triglyceride (oil)**		**Biodiesel**	
	^{1}H (δ, ppm)	**^{13}C (δ, ppm)**	**^{1}H (δ, ppm)**	**^{13}C (δ, ppm)**
Carbonyl (C=O)	–	172.662–173.086	–	174.298
Olefinic protons/carbons (-CH=CH-)	5.329	127.924–130.092	5.333–5.341	127.940–130.164
Methine proton/carbon at C2 of glycerides (-CH-CO_2R)	5.280	68.955	–	–
Methylene protons/carbon at C1 and C3 of glycerides (-CH_2-CO_2R)	4.116–4.324	62.091	–	–
Methoxy protons/carbons (-$COOCH_3$) of esters	–	–	3.657	51.423
Bis-allylic protons/carbon (-C=C-CH_2-C=C-)	2.764	–	2.766	–
α-methylene to ester (-CH_2-CO_2R)	2.303	–	2.294	–
α-methylene to double bond (-CH_2-C=C-)	2.019–2.053	–	2.018	–
β-methylene to ester (CH_2-C-CO_2R)	1.609	–	1.618	–
Backbone methylenes -$(CH_2)_n$-	1.261–1.304	22.658–34.171	1.267–1.306	22.640–34.101
Terminal methyl protons/carbon (C-CH_3)	0.880–0.888	14.12, 14.16	0.881–0.889	14.109, 14.146

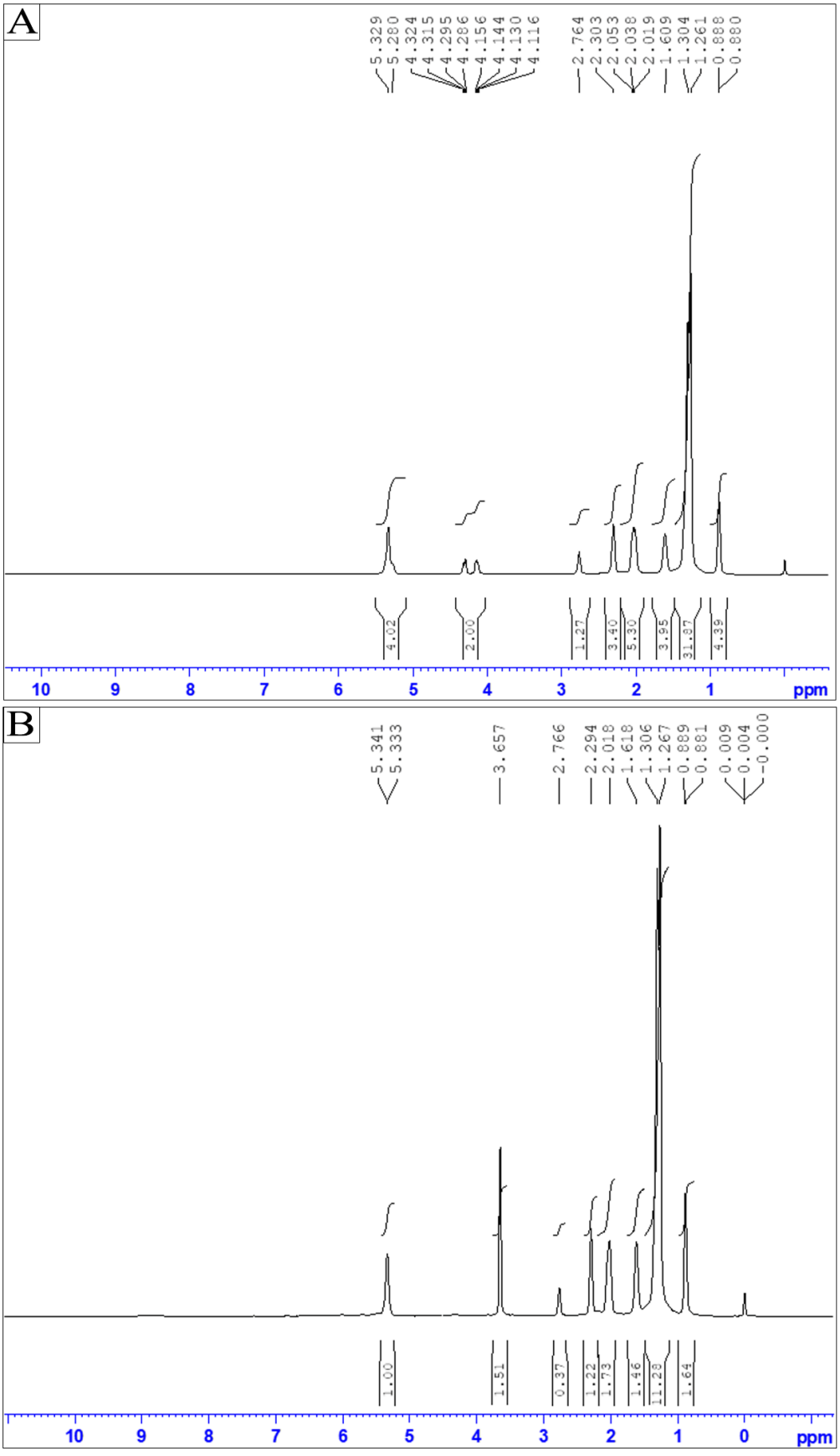

Fig. 2.17. ^{1}H-NMR spectrum of *J. curcas* oil (A) and *J. curcas* biodiesel (B).

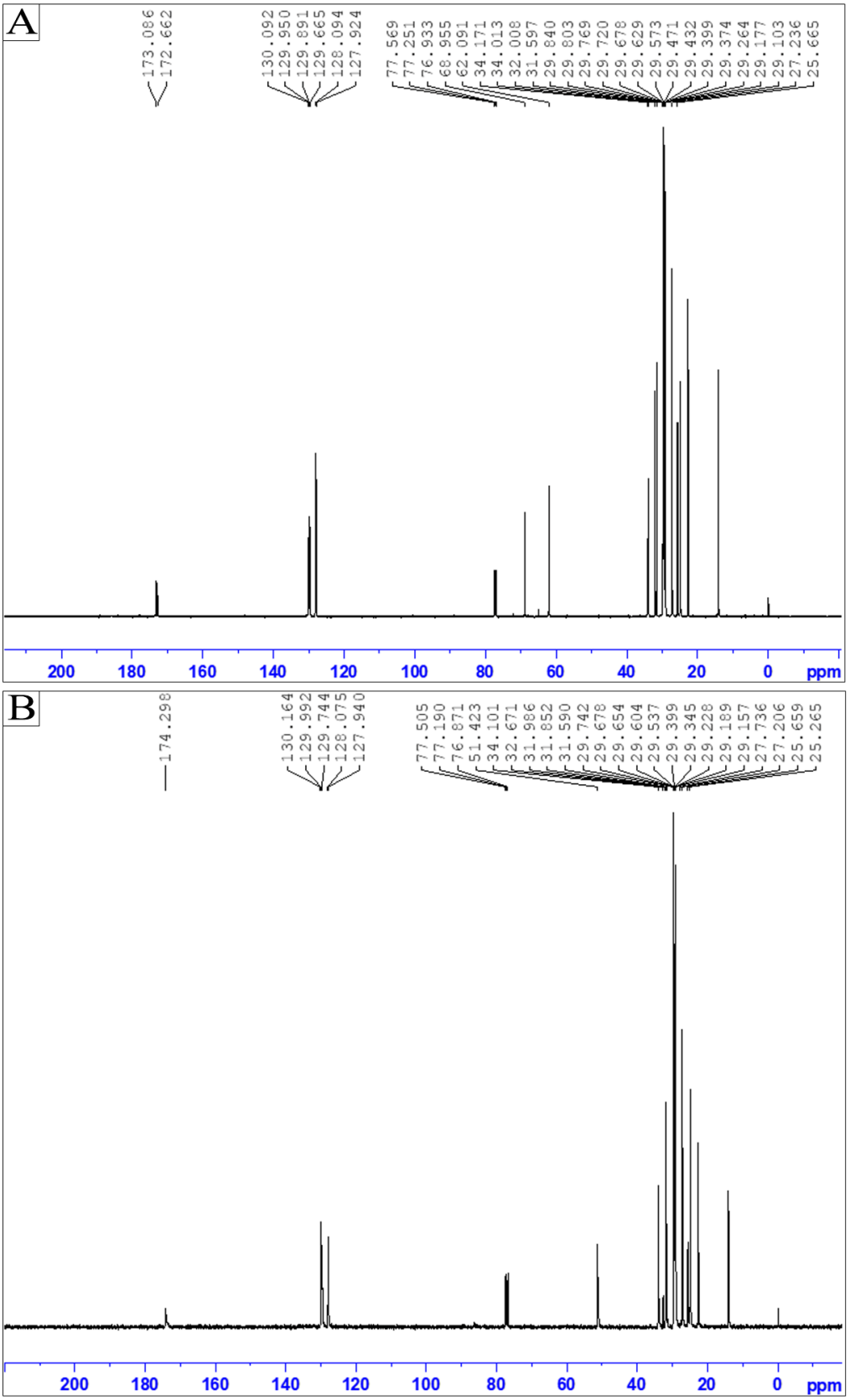

Fig. 2.18. ^{13}C-NMR spectrum of *J. curcas* oil (A) and *J. curcas* biodiesel (B).

2.3.6.3 GC-MS study of *J. curcas* biodiesel

The composition of methyl esters of *J. curcas* biodiesel is analyzed with GC-MS. The GC chromatogram (**Fig. 2.19**) indicated the presence of six different methyl esters of fatty acids and these are shown in **Table 2.6**. The analysis revealed the presence of both saturated and unsaturated fatty acid esters in biodiesel. In this study, methyl oleate is found to be the predominant unsaturated fatty acid methyl ester with 78.648 % followed by saturated fatty acid *viz*. methyl palmitate with 13.489 %. The other unsaturated fatty acid methyl esters were methyl palmitoleate (0.612 %) and methyl gondoate (0.301 %), whereas methyl stearate (5.592 %) and methyl arachidate (0.194 %) were the other saturated fatty acid methyl esters identified in the *J. curcas* biodiesel.

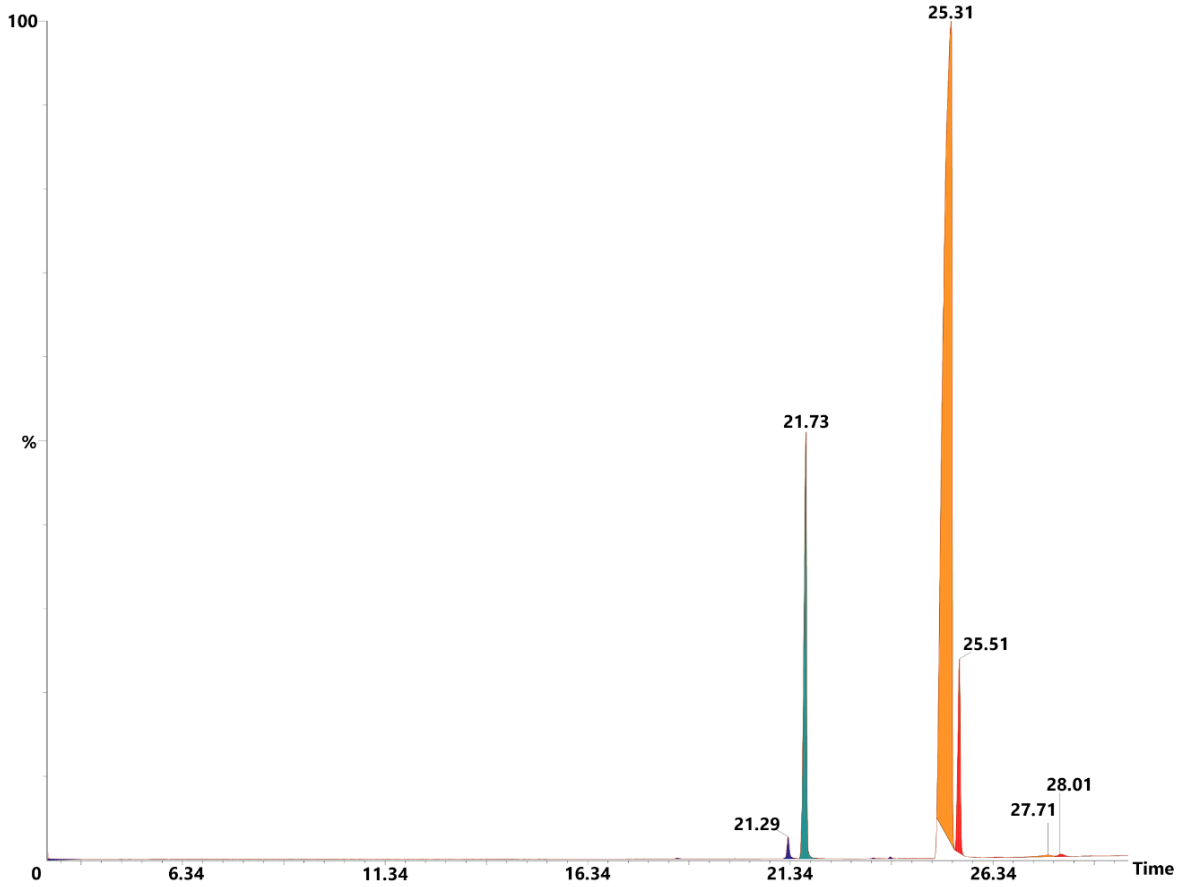

Fig. 2.19. GC chromatogram of *J. curcas* biodiesel produced from *H. fragrans* catalysed transesterification.

Table 2.6: Composition of *J. curcas* biodiesel produced via *H. fragrans* catalysed transesterification

Retention time	Methyl esters (Biodiesel)	Composition (%)
21.29	Methyl palmitoleate [C16:1]	0.612
21.73	Methyl palmitate [C16:0]	13.489
25.31	Methyl oleate [C18:1]	78.648
25.51	Methyl stearate [C18:0]	5.592
27.71	Methyl gondoate [C20:1]	0.301
28.01	Methyl arachidate [C20:0]	0.194

2.3.6.4 *J. curcas* biodiesel properties

The properties of the produced *J. curcas* biodiesel and its comparison are summarized in **Table 2.7**. The density of *J. curcas* biodiesel at 15 ^{o}C was found to be 0.878 g cm^{-3} which is within the recommended range of EN 14214 standard and comparable to that of other biodiesels reported by Chouhan and Sarma [114], Sarma et al. [111], Kumar et al. [197], Deka and Basumatary [11], Basumatary et al. [208] and Gohain et al. [109,220]. In line with the low viscosity which is necessary for favourable combustion characteristics along with non-deposition in the engine, the kinematic viscosity at 40 ^{o}C of the *J. curcas* biodiesel is found to be 3.624 mm^2 s^{-1} which is satisfying the standard limits (**Table 2.7**) and is comparatively lower to the values reported by Chouhan and Sarma [114], Sarma et al. [111], Kumar et al. [197], Adesina et al. [232], Deka and Basumatary [11] and Odude et al. [106]. A cetane number of 55.50 of the present biodiesel was obtained which exceeds the minimum limits of international standards (ASTM D6751 and EN 14214). However, a higher cetane number of 76.93, 61.5 and 64.2 were reported by Adesina et al. [232], Deka and Basumatary [11] and Basumatary et al. [208] for the biodiesel from palm oil, yellow oleander oil and *Gmelina arborea* oil (**Table 2.7**). In this study, the cetane index of biodiesel was calculated and found to be 59.23 which is slightly higher than the experimental value of 55.50. The pour point and cold filter plugging point of *J. curcas* biodiesel were measured as -6 and -3. The saponification value (number) representing the saponifiable unit per unit weight of the biodiesel was obtained as 191.64 mg KOH/g and is comparable with the values reported by Basumatary et al. [208] for *Gmelina arborea* biodiesel (**Table 2.7**).

Table 2.7: Comparison of *properties* of *J. curcas* biodiesel produced *by H. fragrans* catalysed transesterification with standards (ASTM D6751, EN 14214) and reported biodiesel properties

Properties	**ASTM D6751**	**EN 14214**	**Jatropha biodiesel (This work)**	**Reported biodiesel**								
				Jatropha oil [114]	**Jatropha oil** [111]	**Jatropha oil** [197]	**Palm oil** [232]	**Yellow oleander oil** [11]	**Palm oil** [106]	***Gmelina arborea* oil** [208]	**WCO** [109]	**WCO** [220]
Density (15 ^{o}C, g/cm^{3})	NS	0.86–0.90	0.878	0.891	0.875	0.875	-	0.875	-	0.877	0.89	0.87
Kinematic viscosity (40 ^{o}C, mm^{2}/s)	1.9–6.0	3.5–5.0	3.624	6.8	5.7	4.75	4.3	4.33	4.7	-	3.12	3.10
Cetane number	47 (min)	51 (min)	55.5	-	48.6	48.3	76.93	61.5	44.4	64.2	55	57
Cetane index	NS	NS	59.23	-	-		-	62.9	-	-	-	-
Pour point (^{o}C)	NS	NS	-6	-	3	-6	-6	3	-3	-	-9	-10
CFPP (^{o}C)	NS	NS	-3	-	-	-	-	6	-	-		-
Saponification number (mg KOH/g)	NS	NS	191.64	-	-	-	-	-	-	185.7	-	-

Iodine value (g I_2/100 g)	NS	120 (max)	69.11	-	119	74.5	40.90	69.9	24.7	51.0	-	-
API	36.95	NS	34.28	0.892	0.875	-	32.42	-	30.51	-	-	-
Diesel index	50.4	NS	68.37	-	-	-	92.95	-	47.87	-	-	-
Aniline point	331	NS	199.47	-	-	-	-	-	-	-	-	-
HHV (MJ/kg)	NS	NS	40.53	37.1	39.25	38.35	-	44.986	-	40.7	40.20	40.30

Min–minimum; max–maximum; NS–not specified; CFPP–cold filter plugging point; API–American petroleum index; HHV–higher heating value (calorific value).

The iodine value indicating the degree of unsaturation of the biodiesel was found to be 69.11 g I_2/100 g, which is below the specified maximum limit of 120 (EN 14214 standard) and comparable to the results reported by Deka and Basumatary [11] for yellow oleander biodiesel (69.9 g I_2/100 g) and Kumar et al. [197] for *J. curcas* biodiesel (74.5 g I_2/100 g). Higher iodine value of 119 g I_2/100 g was reported in the work of Sarma et al. [111]. The American petroleum index, diesel index and aniline point of the present biodiesel were determined to be 34.28, 68.37 and 199.47, respectively. The higher heating value (calorific value) of the present biodiesel is resulted to be 40.53 MJ/kg, which is well comparable to that of the reported biodiesels (**Table 2.7**).

2.4 Conclusion

In this study, a highly efficient basic heterogeneous catalyst from *H. fragrans* could be developed for the effective synthesis of *J. curcas* biodiesel. The catalyst CC-550 is exhibiting better performance in catalysis with a maximum biodiesel yield of 97.75 % in 65 min with TOF of 35.55 min^{-1} compared to the CC-850 (96.58 %) and BHC (96.61 %) with TOF of 27.71 and 29.47 min^{-1}, respectively under the ORCs of 12:1 MTOR and 7 wt.% of catalyst loading at 65 ^oC. The CC-550 displayed higher basic character (pH value of 12.89 at 1:5 w/v) due to its high K content (19.05 wt.% in EDX, 15.19 atomic % in XPS) and the K as an active species in the form of K_2CO_3 and K_2O played the key role for the excellent efficiency in the catalysis of biodiesel production. Hammett method showed stronger basicity of CC-550 (0.423 mmol/g) representing the better efficacy for the catalysis. The catalyst could produce a high biodiesel yield of 90.22 % even in the 3rd cycle of reaction under the ORCs. The low Ea value of 32.31 kJ mol^{-1} is indicating the simplicity of the reaction and the frequency factor is found to be 1.155×10^7 min^{-1}. The *H. fragrans* catalyst prepared from renewable and inexpensive raw materials is an environment-friendly and excellent catalyst with ease of handling for the base-catalysed reaction which has a strong potential for large-scale and cost-effective applications in the synthesis of biodiesel.